Towards accurate calculation of supercapacitor electrical variables in constant power applications using new analytical closed-form expressions

Martin Ćalasan [a], Ahmed F. Zobaa [b,*], Hany M. Hasanien [c], Shady H. E. Abdel Aleem [d], and Ziad M. Ali [e, f]

[a] Faculty of Electrical Engineering, University of Montenegro, Montenegro

[b] College of Engineering, Design & Physical Sciences, Brunel University London, Uxbridge, United Kingdom

[c] Electrical Power and Machines Department, Faculty of Engineering, Ain Shams University, Cairo 11517, Egypt

[d] Electrical Engineering Department, Valley Higher Institute of Engineering and Technology, Science Valley Academy, Qalyubia, Egypt

[e] Electrical Engineering Department, College of Engineering at Wadi Addawaser, Prince Sattam bin Abdulaziz University, Saudi Arabia

[f] Electrical Engineering Department, Aswan Faculty of Engineering, Aswan University, Egypt

[*] Corresponding author

E-mail addresses: martinc@ucg.ac.me (M. Ćalasan), azobaa@ieee.org (A. Zobaa), hanyhasanien@ieee.org (H. Hasanien), engyshady@ieee.org (S. Abdel Aleem), and dr.ziad.elhalwany@aswu.edu.eg (Z. Ali).

Abstract

Supercapacitor (SC) is one of the most trending energy storage solutions. The SCs equivalent circuit models have been extensively applied to energy management because of their accuracy and simplicity. However, there is a difficulty in solving the conventional differential equation-based model used to characterize the electrical behavior of SCs operating in constant power applications. Hence, numerical or metaheuristic techniques have been used in the literature to derive SC's internal voltage at any time. In this work, a thorough mathematical analysis that enables a precise calculation of the electrical variables implied in the charge/discharge processes of SCs operated at constant power as a function of time is presented. First, the transcendental discharge voltage expression of SCs operating at constant power is formulated, and then it was solved using the Special Trans Function theory (STFT). The precision of calculation of the method used for solving the transcendental expression is presented and discussed. Second, the transcendental voltage of charging expression of SCs operating at constant power as a function of time is also formulated, and then it was solved using Lambert W equation. Third, a comparison of different methods for solving mentioned equations is presented. Fourth, the electrical variables involved in the charge/discharge processes of SCs – voltage, current, power, energy, state of charge, and power loss are investigated. Furthermore, the results obtained for the variation of parameters and their operating conditions demonstrate the proposed equations' applicability and accuracy. Finally, the results obtained validate that the closed-form expressions suggested in this paper are accurate and straightforward, which can contribute to proper modeling, investigation, sizing, regulation, and control of constant power SCs in modern energy systems.

Keywords— Charge and discharge processes; constant power applications; Lambert W function; mathematical analysis; parameter estimation; supercapacitors; transcendental equations.

Abbreviations

PECE	Predictor-corrector method
RC	Series-connected resistance (R) and capacitance (C) that represents the SC model
RESs	Renewable energy sources
SC	Supercapacitor
SoC	State of charge
TS	Taylor series
STFT	Special Trans Function Theory

Nomenclature

a	Arbitrary positive real number
C	Capacitance of the SC (kF)
$E_{discharge}$	Discharge energy (J)
E_{stored}	Energy stored in the SC (J)
i	Discharge current (A)
$G_{>}$ and $G_{<}$	Error functions
M	Positive integer
R	Internal resistance of the SC (mΩ)
P	Constant power (W)
P_{loss}	Power losses of the SC
P_r	Calculation precision
t	Time needed by the internal voltage to reach a current value from the initial one (ms)
u	Internal voltage (v)
U_0	Initial starting voltage
u_{co}	External voltage (v)
[x]	The largest integer that is less than or equal to x
α	Coefficient of the transcendental expression of the SC charge equation
β	Coefficient of the transcendental expression of the SC discharge equation
θ	Variable of the transcendental expression of the SC discharge equation
Ψ	Variable of the transcendental expression of the SC charge equation

1. Introduction

Energy generation from renewable energy sources (RESs) is emerging across the world rapidly in response to technical, economical, environmental, political, and social requirements under the umbrella of curbing the usage of high-carbon conventional fossil energy resources to droop the increasing rate of global warming [1]. However, many factors affect the operation of modern power systems with high penetration of RESs, such as the intermittent nature of renewables and geographic constraints, and incomplete flexibility for power system operators to reduce frequency fluctuations and balance generation and demand in the long term [2], particularly with the increased RESs share in global energy markets. Therefore, there is an imperative need to store energy using the developing energy storage (ES) technologies [3], [4]. There is no doubt that ES is the primary driver towards achieving emission-free power generation that can accelerate the conversion of energy systems from fossil fuel-based sources to renewable-based sources [5], [6].

In the broadest sense, energy storage is one of the good facilities that can increase resiliency and enhance reliability of modern energy systems and enable the integration of clean renewable energy sources into these systems. Many ES technologies with various energy capacities that rely on chemical, thermal, electrical, mechanical, or electrochemical solutions can be connected to energy systems [7]. One of the most interesting ES applications that need rapid charge/discharge cycles is the supercapacitors (SCs). They are a particular type of capacitors with a capacitance value much higher than the traditional capacitors [8]. SCs can store 10 to 100 times more energy per unit volume than electrolytic capacitors, accept charge much faster than any batteries [9], [10]. SCs are frequently used to improve power quality, afford backup power, and support voltage since their long cyclability, high efficiency, and rapid response characterize them [5]. For instance, they are widely employed in several applications such as hybrid electric vehicles [11], induction generators and energy storage applications [12], [13], power supplies [14], wireless sensors nodes [15], [16], oscillator circuits [17] and others. However, SCs have a lower voltage limit and are characterized by low energy density and high self-discharge loss and cost [5]. Because the research interest in SC modeling is growing, accurate SC models are essential for developing management systems to investigate electrical, aging, and thermal concerns accurately [18]. So, it is imperative to form a simple but accurate mathematical model to simulate the SC's performance [19].

In the available literature, several models of these devices have been developed [18]. From the electrical perspective, in [18], Zhang et al. presented an overview of various SC models – electrochemical, equivalent circuit, intelligent-based, and fractional-order. The equivalent SC models of Zhang are widely recognized and used due to their simplicity and accuracy. Moreover, comprehensive research about SC models was offered by Grbovic et al. in [20]. Unlike Zhang et al.'s investigation, Grbovic et al. in [20] have treated the SC as a varying capacity. Hereafter, the third usually used model for SC representation was presented by Musolino et al. in [21]. However, Musolino SC models are complex as they consider many factors to parameterize low and high-frequency currents' effects on SC cells.

A series-connected resistance (R) and capacitance (C) represent the classical SC model, known as the RC model [22–24], which is widely used in all studies dealing with the charge and discharge process of the SC. Some research works have promoted an adapted SC model by including a parallel resistance to account for the leakage current [25]; it can be used when the self-discharge phenomenon is the primary motivator. It can be concluded that the RC model modification does not significantly impact the model accuracy, although it gives a better SC representation. What makes the SC modeling problem more difficult is unknown or missing parameters or the incomplete data in the datasheets offered by the vendors and manufacturers. Also, sometimes, SC parameters can be found in the manufacturer datasheet, but it is needed to estimate them based on other data or certain operating conditions [26]. This is why it is not simple to model the SC characteristics precisely with the missing data. However, the positive point that strengthens the use of the RC model is that its parameters could be considered constant in normal operating conditions, particularly the temperature, without significant errors [27], [28]. SCs usually operate in the charge/discharge process at constant current, impedance, and power [29]. The time-domain analytical expressions for all electrical characteristics of SCs under these modes of operations are presented in [29]. However, SCs have been used in most practical applications through the charge/discharge process at constant power or constant current [26]. In this regard, because the RC-based models in constant power applications have a complex mathematical solution, the authors in [29] have solved the SC modeling problem numerically using the predictor-corrector (PECE) method. Namely, the mentioned method extends Adams-Bashforth-Moulton's procedure for solving ordinary differential equations by fractional differential derivatives [30]. Closed-form expressions of SC electrical variables using Lambert W function in constant power applications are presented by Joaquín Pedrayes et al. in [26]. Both charge and discharge processes are formulated using the Lambert W function without solving complex differential equations. However, the discharge process results are only presented. Much additional mathematical formulation is given and added in the mathematical representation of this process, complicating its entire screen. Furthermore, no comments were made or discussed on the analytical solution of the proposed equations. Moreover, both charge and discharge processes were presented in terms of the standard Lambert W function without sufficient feedback on the solutions' number, accuracy, and complexity.

In this paper, a thorough mathematical time-domain analysis that enables a precise calculation of all electrical variables involved in charge/discharge processes of SCs (voltage, current, power, and energy) operated at constant power is presented. Knowing the time-current and time-voltage (and vice-versa) curves during charge or discharge processes of SCs, accurate information can be obtained on SC's voltage value or SC's value at any time interval. These expressions can be useful in control loops where it is needed to control the value of current/voltage during the charge/discharge process of SCs or to calculate the SC's internal voltage value at any time. The proposed analytical closed-form expressions permit a direct calculation of all electrical variables involved in charge/discharge processes of SCs as a function of time, in addition to permit calculating the interrelations between these electrical variables in a straightforward matter, which can advance a good base for proper modeling, investigation, sizing, regulation, and control of constant power SCs in modern energy systems.

Mathematically speaking, the discharge process of SCs operating at constant power can be represented as a function of the type $x=\beta(\exp(x))$. This equation has two solutions. However, taking into account the physical constraints, only one is acceptable. Also, the charging process of SCs operating at constant power can be represented as a function of the type $z=\alpha(\exp(-z))$, which also has one solution. In this regard, both the derived transcendental equations and corresponding expressions for electrical variables involved in SCs' charge/discharge processes in constant power applications as a function of time are solved analytically. The mathematical expressions derived are accurate and straightforward and do not require any other mathematical formulations. Furthermore, a comparison of different methods for solving mentioned equations is presented.

The rest of the work is organized as follows: In Section 2, a mathematical analysis of SCs that operate in constant power applications is presented. The proposed analytical methods for solving transcendental equations that describe both charge and discharge processes are presented and discussed in Section 3. A comparison of different methods for solving mentioned equations is presented. Results of the charge-discharge operations are presented and discussed in Section 4. Other key performance metrics as the state of charge (SoC) and power loss (P_{loss}), are derived in different operating conditions, and the results are visualized. Lastly, the concluding notes and future work directions are given in Section 5. This paper also includes an appendix to show how the closed-form expressions derived in this contribution were solved

(Mathematica codes for expressing the discharging and charging processes of a SC at constant power), which may be valuable for researchers who want to develop a model of SCs operating in constant power applications.

2. Mathematical investigation and analysis of supercapacitors operated at constant power

The conventional RC model of the SC comprises a capacitance C, internal resistance R, discharged at constant power P as illustrated in Fig. 1 [26]. In this figure, u denotes the internal voltage, u_{co} denotes the external voltage, while i denotes the discharge current.

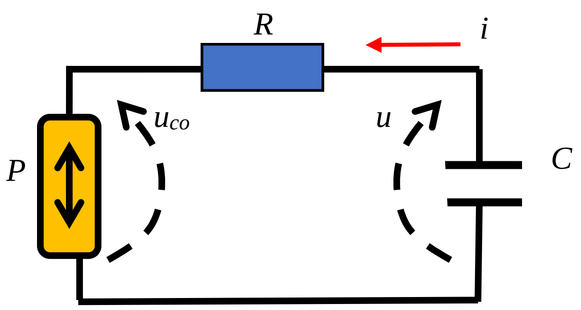

Fig. 1. Discharge of a SC at constant power (P).

In the mathematical sense, the power balance equation of this model can be described as follows:

$$P + Ri^2 = ui \tag{1}$$

where P>0 in the discharge process and P<0 in the charge one.

2.1 Discharge process of a SC at constant power

The internal voltage (u) of the SC bank can be represented as follows:

$$u = u_{co} + Ri \tag{2}$$

Taking into account the relation between the current and voltage of the SC bank, one can find that:

$$u' = \frac{du}{dt} = -\frac{i}{C} \tag{3}$$

Eq. (3) can be expressed in terms of Eq. (1); thus:

$$u'^2 + \frac{u}{RC}u' + \frac{P}{RC^2} = 0 \tag{4}$$

Even though Eq. (4) has two solutions, only one solution is acceptable, which is the positive one; thus:

$$u' = -\frac{u}{2RC} + \frac{\sqrt{u^2 - 4PR}}{2RC} \tag{5}$$

Solving Eq. (5) to get the time t needed by the internal voltage u to reach a current value, from initial voltage U_0, has the following expression:

$$t = \frac{C}{4P}\left(U_0^2 + U_0\sqrt{U_0^2 - 4PR} - u^2 - u\sqrt{u^2 - 4PR} - 4PR\log\left(\frac{U_0 + \sqrt{U_0^2 - 4PR}}{u + \sqrt{u^2 - 4PR}} \right) \right) \tag{6}$$

From the previous equation, Eq. (6), the following u expression can be derived. Thus:

$$u^2 + u\sqrt{u^2 - 4PR} - 4PR\log\left(u + \sqrt{u^2 - 4PR} \right) = h \tag{7}$$

where

$$h = U_0^2 + U_0\sqrt{U_0^2 - 4PR} - 4PR\log\left(U_0 + \sqrt{U_0^2 - 4PR} \right) - \frac{4Pt}{C} \tag{8}$$

From the previous equations, Eqs. (7) and (8), u expression can be formulated as a transcendental equation as follows:

$$\theta = \beta\exp(\theta) \tag{9}$$

where

$$\beta = \frac{1}{4PR}\exp\left(\frac{2PR - h}{2PR} \right) \tag{10}$$

Hence, the voltage expression can be written as follows:

$$u = \sqrt{PR}\left(\frac{1 + \theta}{\sqrt{\theta}} \right) \tag{11}$$

Derivation of Eq. (11) is explained in detail in Appendix A. It should be noted that transcendental expression $\theta = \beta\exp(\theta)$ has two solutions [31]. One of the solutions is less than 1, denoted as $\theta_<$, and the second solution is greater than 1, denoted as $\theta_>$. Both solutions are illustrated in Fig. 2.

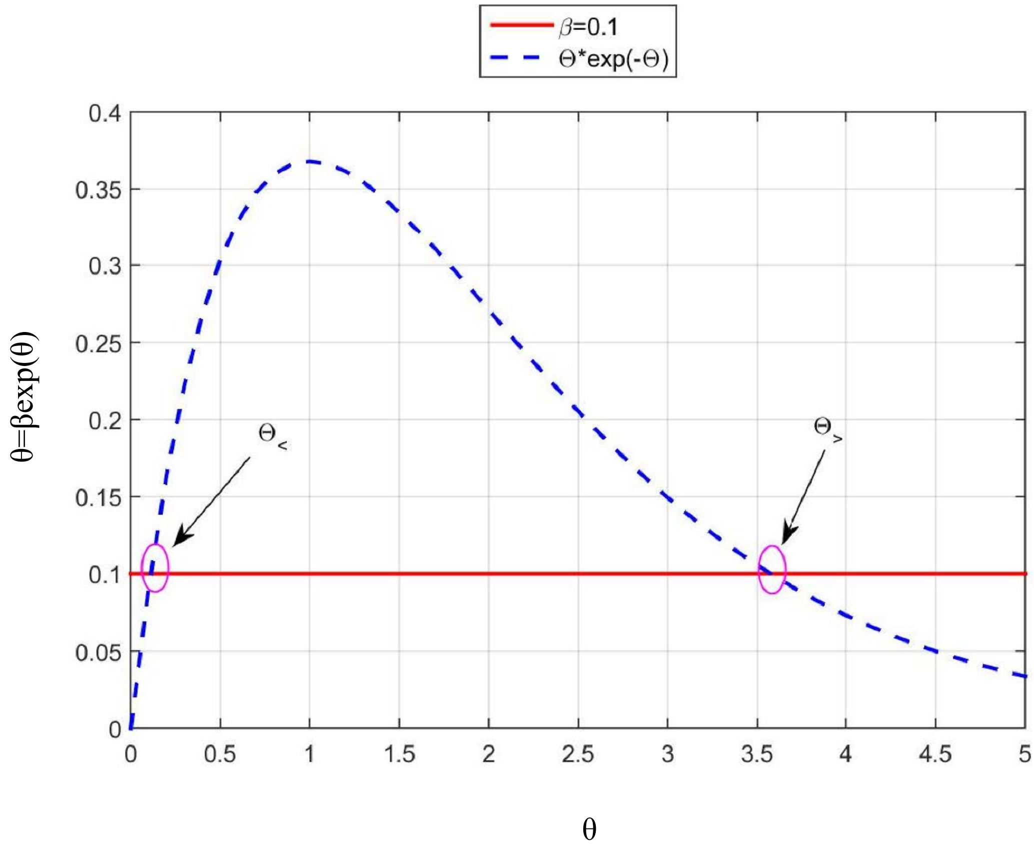

Fig. 2. Graphical representation of solutions of the transcendental expression $\theta = \beta \exp(\theta)$.

During the discharge process, i.e., $P>0$, the voltage decreases. On the other side, observing the hth equation (Eq. (8)), it can be seen that h decreases with the rise in time. In this case, the coefficient β increases. Hence, by observing Fig. 2, it can be seen that with the increase in coefficient β, we can find a rise in $\theta_<$ and a decrease in $\theta_>$. Solution $\theta_<$ ranges between 0 and 1, while $\theta_>$ is greater than 1. Observing the graph for u as a function of θ shown in Fig. 3, it can be seen that a decrease in θ causes the reduction in u for $\theta_>$. Therefore, it is clear that for the discharge process, we should consider the solution $\theta_>$.

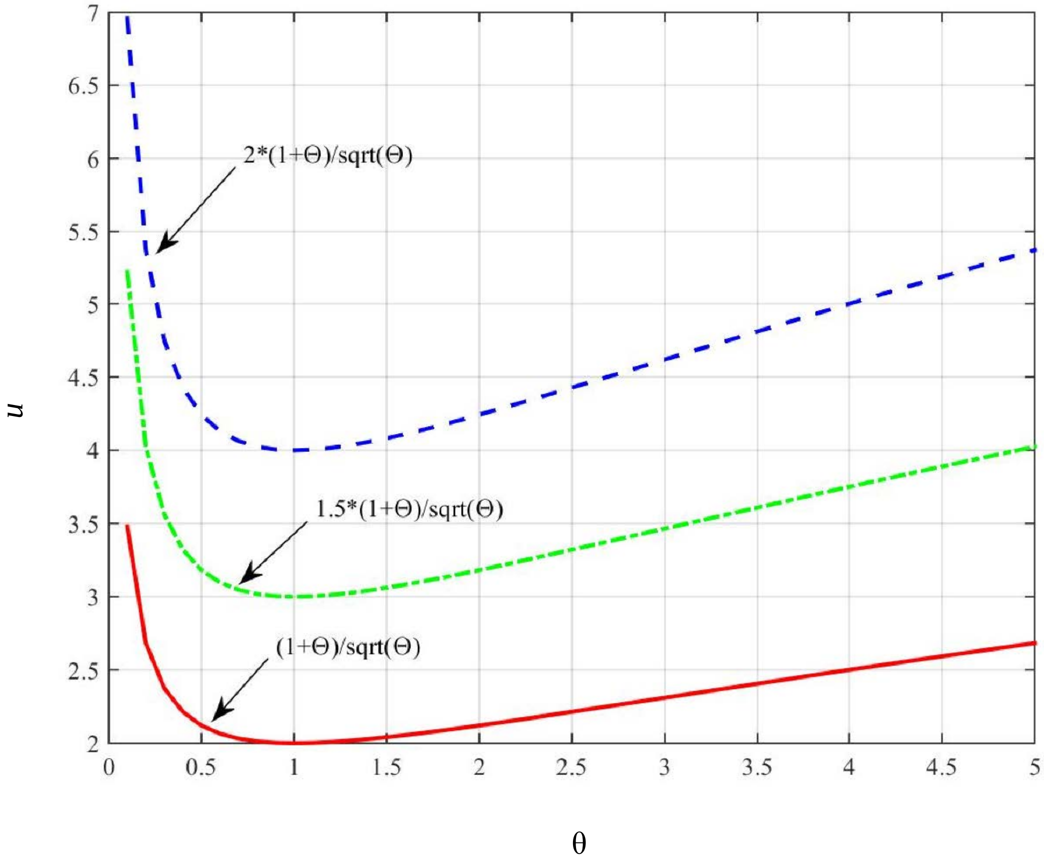

Fig. 3. Variation of the voltage u versus θ

The discharge current can be calculated in the following manner:

$$i = C\left(\frac{du}{dt}\right) = C\left(\frac{du}{d\theta}\right)\left(\frac{d\theta}{dt}\right) \tag{12}$$

After some mathematical manipulations, the mathematical expression for the current is derived as follows:

$$i = \sqrt{\frac{P}{R\theta}} \tag{13}$$

Derivation of Eq. (13) is explained in detail in Appendix A.

Eqs. (14) and (15) represent the derived closed-form expressions of the instantaneous energy stored in the SC (E_{stored}) and the energy discharged ($E_{discharge}$), respectively.

$$E_{stored} = \frac{1}{2}\left(Cu^2\right) = \frac{1}{2}C\left(\sqrt{PR}\,\frac{1+\theta}{\sqrt{\theta}}\right)^2 = \frac{PRC}{2}\left(2+\theta+\frac{1}{\theta}\right) \tag{14}$$

$$E_{discharege} = \frac{1}{2}C\left(U_0^2 - u^2\right) = \frac{PRC}{2}\left(\frac{U_0^2}{PR} - 2 - \theta - \frac{1}{\theta}\right) \tag{15}$$

2.2 Charge process of a SC at constant power

During a charging process, the power is less than zero, i.e., $P<0$. Hence, it can be considered that $P_1=-P$, and the following expressions can be deduced:

$$h = U_0^2 + U_0\sqrt{U_0^2 + 4P_1R} + 4P_1R\log\left(U_0 + \sqrt{U_0^2 + 4P_1R}\right) + \frac{4P_1t}{C} \tag{16}$$

Also, we can write the following:

$$u^2 + u\sqrt{u^2 + 4P_1R} + 4P_1R\log\left(u + \sqrt{u^2 + 4P_1R}\right) = h \tag{17}$$

Eq. (17) can be transformed to the following form:

$$\Psi = \alpha\exp\left(-\Psi\right) \tag{18}$$

Eq. (18) has one acceptable solution. In which the coefficient α is given as

$$\alpha = \frac{1}{4P_1R}\left[\exp\left(\frac{2P_1R + h}{2P_1R}\right)\right] \tag{19}$$

Therefore, the voltage u can be derived as follows:

$$u = \sqrt{P_1R}\,\frac{\Psi - 1}{\sqrt{\Psi}} \tag{20}$$

Finally, the mathematical expression for the charge current i is derived as follows:

$$i = \sqrt{\frac{P_1}{R\Psi}} \tag{21}$$

Derivations of Eqs. (20) and (21) are explained in detail in Appendix A.

3. Proposed analytical solutions

The proposed methods for solving the transcendental equations representing charge and discharge are presented and discussed in this section. A comparison of different methods for solving the obtained equations is presented.

3.1 Analytical solutions of the discharging equation of the SC at a constant power

The transcendental expression $\theta = \beta\exp\left(\theta\right)$ can be solved using the Special Trans Function theory (STFT) [31], [32]. The lower value of the solution ($\theta_<$) has the following form:

$$\left\langle \theta_< \right\rangle_{P_r} = \sum_{n=0}^{[x]} \left(-1\right)^n \frac{\beta^n \left(x-n\right)^n}{n!} \tag{22}$$

where [x] denotes the largest integer that is less than or equal to x, while P_r represents calculation precision.

The value of the higher solution ($\theta_>$) can be calculated as follows:

$$\langle \theta_> \rangle_{P_r} = \langle \theta_< \rangle_{P_r} + K \tag{23}$$

where

$$K = \log\left(\frac{F_>(\beta, u-a)}{F_>(\beta, u)} \right) \tag{24}$$

$$F_>(\beta, u) = bR(b,u)\exp(bu) + R'(b,u)\exp(bu) \tag{25}$$

So that

$$\begin{aligned} R(b,u) &= \sum_{n=0}^{[u/a]} (-1)^n \frac{\left(b\exp(-ab)\right)^n (u-na)^n}{n!} \\ R'(b,u) &= -b\exp(-ab)R(b,u-a) \end{aligned} \tag{26}$$

$$b = \frac{\theta_<}{a} \tag{27}$$

In the previous equation, Eq. (27), a is an arbitrary positive real number.

The accuracy of the calculation can be expressed in the following manner for both solutions:

$$\begin{aligned} P_{r>} &= \left|1 - \log(G_>)\right| \\ P_{r<} &= \left|1 - \log(G_<)\right| \end{aligned} \tag{28}$$

where the error functions $G_>$ and $G_<$ can be calculated as follows:

$$\begin{aligned} G_> &= \left|\theta_> - \theta_>\left(exp(\theta_>)\right)\right| \\ G_< &= \left|\theta_< - \theta_<\left(exp(\theta_<)\right)\right| \end{aligned} \tag{29}$$

The solutions of the equation $\theta = \beta\exp(\theta)$ are presented in Table 1. Also, the solutions obtained are shown in Table 2 in terms of accuracy P_r. It can be noted that for all the considered values of β, the calculation error is very small, or approximately zero, particularly because of the kind of physical problem solved in this work.

Table 1. Solutions obtained for $\theta = \beta \exp(\theta)$ at x=100

β	$\theta_<$	$G_<$	u	$\theta_>$	$G_>$
1/10	0.111832559158962965	1.056×10^{-152}	100a	3.5771520639572	9.863×10^{-38}
			200a		1.075×10^{-75}
			300a		9.885×10^{-114}
1/5	0.259171101819073745	5.600×10^{-101}	100a	2.54264135777352	2.373×10^{-51}
			150a		5.471×10^{-77}
			200a		5.514×10^{-100}
1/3	0.619061286735945112	1.696×10^{-40}	20a	1.5121345516578	7.876×10^{-15}
			50a		9.492×10^{-37}
			150a		4.145×10^{-40}

3.2 Analytical solutions of the charging equation of the SC at a constant power

The graphical representation of the equation $\Psi = \alpha \exp(-\Psi)$ is presented in Fig. 4. The transcendental expression $\Psi = \alpha \exp(-\Psi)$ represents the well-known Lambert W equation [33–36]. The conventional methods for solving the Lambert W function are numerical and iterative. The numerical methods are presented in many different domains (for example, Fritsch's iteration, Halley's iteration, etc.). The iterative techniques, unlike analytical solutions, are somewhat complicated.

Table 2. Solutions obtained in solving $\theta = \beta \exp(\theta)$ at x=100 in terms of P_r

β	x	$P_{r<}$	u	$P_{r>}$
1/200	100	321	100a	16
			200a	30
			300a	47
	200	637	100a	16
			200a	30
			300a	47
	300	953	100a	16
			200a	30
			300a	47
1/100	100	285	100a	19
			200a	38
			300a	56
	200	566	100a	19
			200a	38
			300a	56
	300	846	100a	19
			200a	38
			300a	56
1/10	100	153	100a	38
			200a	76

β	x	$P_{r<}$	u	$P_{r>}$
			300a	115
	200	303	100a	38
			200a	76
			300a	115
	300	453	100a	39
			200a	76
			300a	115
1/4	100	80	100a	59
			200a	117
			300a	176
	200	157	100a	59
			200a	117
			300a	176
	300	236	100a	59
			200a	117
			300a	176

Numerous program packages, such as Python, Mathematica, MATLAB, Maple, and others, have developed a solver for solving the Lambert W function. For instance, the Lambert W function is implemented as *LambertW* in Maple, *lambertw* in Matlab, Python, Octave, *lambert_w* in Maxima, and *ProductLog* in Mathematica. The main drawback of all the implemented solvers is that they do not enable control of solution accuracy.

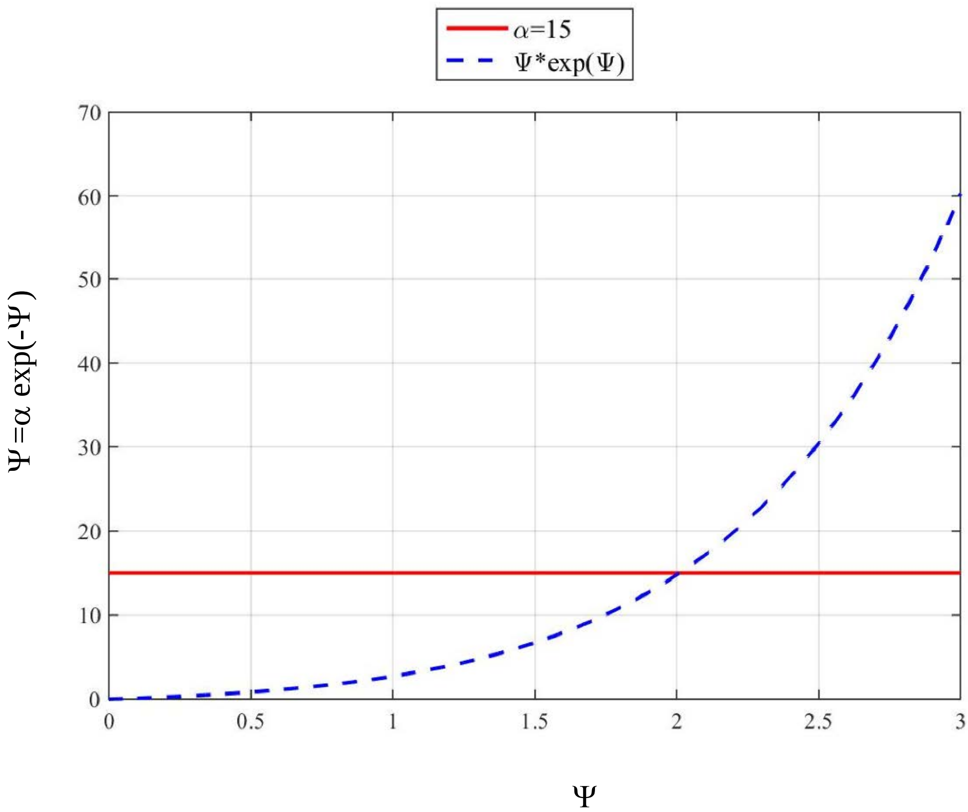

Fig. 4. The graphical representation of equation $\Psi = \alpha \exp(-\Psi)$

Two analytical methods for solving the Lambert W function can be found in the literature. The first method is based on the Taylor series (TS) usage, while the second is based on the use of STFT [34,36]. The TS of W_0 around 0 can be found using the Lagrange inversion theorem as follows:

$$W(\alpha)=\sum_{n=1}^{\infty}\frac{(-n)^{n-1}}{n!}\alpha^{n} \tag{30}$$

For practical implementation and simplicity, Eq. (30) can be rewritten in the following form:

$$W(\alpha)=\sum_{n=1}^{M}\frac{(-n)^{n-1}}{n!}\alpha^{n} \tag{31}$$

where M represents a positive integer.

For a large value of α, an asymptotic formula for solving the Lambert W equation will have the following formulation:

$$\begin{aligned}W(\alpha)&=L_1-L_2+\sum_{l=0}^{\infty}\sum_{m=1}^{\infty}\frac{(-1)^{l}\begin{bmatrix}l+m\\ l+1\end{bmatrix}}{m!}L_1^{-l-m}L_2^{m}\\ &=L_1-L_2+\frac{L_2}{L_1}+\frac{L_2(-2+L_2)}{2L_1^2}+\frac{L_2\left(6-9L_2+2L_2^2\right)}{6L_1^3}+\dots\end{aligned} \tag{32}$$

where L_1=ln(B) and L_2=ln(ln(α)), $\begin{bmatrix}l+m\\ l+1\end{bmatrix}$ are non-negative Stirling numbers of the first kind [36].

Eq. (18) can also be solved by using STFT [36], in which the solution can be written as follows:

$$\Psi=\alpha\frac{\sum_{n=0}^{M}\frac{\alpha^{n}(M-n)^{n}}{n!}}{\sum_{n=0}^{M+1}\frac{\alpha^{n}(M+1-n)^{n}}{n!}} \tag{33}$$

Hence, to solve Eq. (18), Eqs. (31) – (33) can be used, in which the calculation error (G) can be represented as follows:

$$G=\left|\Psi-\alpha e^{-\Psi}\right| \tag{34}$$

The precision P_r reflects the accuracy. The accuracy of the solution is high for the high values of P_r, in which P_r is defined as:

$$P = \left|1 - \log\left(G\right)\right| \tag{35}$$

In order not to lose generality, specific examples of solving the Lambert equation using Eqs. (31) and (32) are presented in Tables 3 and 4 for different values of α. In this calculation, *Mathematica* is used to solve the equations. The realized *Mathematica* code based on the previously noted equations is given in Appendix B. Based on the presented results, it can be concluded that a higher value of the integer M results in a higher precision of calculations. Higher accuracy can also be obtained if STFT is used to solve the Lambert equation. However, for considerable values of α, using Eq. (33) is the best choice.

To sum up, all of the tested methods for Lambert W solving have good accuracy. Furthermore, for small values of α, this accuracy is extremely high for both STFT and TS. On the other side, for a higher value of α, the asymptotic formula has better accuracy. Because of the physical nature of the problem solved in this work, both methods can be effectively used.

4. Numerical results and discussion

The electrical parameters used in this case study for the discharge and charge processes of a SC at constant power are presented in Table 5, where U_0 denotes the initial starting voltage used.

Table 3. Solutions of Eqs. (31) and (33) for small values of α

α	M	Ψ	G_{STFT}	G_{TAYLOR}
1e^{-6}	3	9.9999900000149999 7333338541655866	4.16×10^{-32}	2.66×10^{-24}
	10		2.50×10^{-80}	6.49×10^{-64}
	20		1.58×10^{-152}	5.44×10^{-120}
	35		7.41×10^{-261}	7.94×10^{-204}
	50		3.09×10^{-369}	1.54×10^{-287}
0.001	3	0.0009990014973385 3088995782787410	4.13×10^{-17}	2.66×10^{-12}
	10		1.66×10^{-44}	6.50×10^{-31}
	20		4.95×10^{-85}	5.45×10^{-57}
	35		3.17×10^{-144}	7.95×10^{-96}
	50		4.66×10^{-204}	1.53×10^{-134}
0.02	3	0.0196115893374056 2729168248268298	1.13×10^{-10}	4.18×10^{-7}
	5		1.11×10^{-15}	6.75×10^{-10}
	10		2.33×10^{-26}	1.36×10^{-16}
	30		7.91×10^{-80}	1.48×10^{-42}
	50		2.21×10^{-120}	3.58×10^{-60}
0.3	5	0.2367553107885593	3.91×10^{-8}	5.93×10^{-3}

	10	1687136699131310	8.36×10^{-16}	8.31×10^{-4}
	50		1.06×10^{-67}	8.22×10^{-8}
	100		4.75×10^{-134}	1.15×10^{-12}
	200		3.09×10^{-266}	1.49×10^{-22}

Table 4. Solutions of Eqs. (32) and (33) for large values of α

α	M	Ψ	P_{STFT}	$P_{ASYMPTOTIC\_FORMULA}$
100	30	3.38563014029005018 48882443645297	8	8
	60		15	13
	100		25	20
	300		74	50
	500		122	80
1000	50	5.24960285240159622 71260563196973	7	24
	100		15	43
	150		22	63
	200		29	82
	250		37	102
10000	60	7.2318460380933727 064756185001412538 840306	5	38
	90		8	55
	120		11	72
	150		14	89
	210		19	122
100000	100	9.28457142862210898 3205132234759581939 3169616724220653050 6106135740393299602 2127668743	6	74
	120		7	87
	140		9	101
	160		10	115
	180		11	125

Table 5. Electrical parameters of the SC

U_0 (V)	C (kF)	R (mΩ)
2.7	1.2	0.58

Table 6 shows the values of the coefficients β, θ as well as the voltage u, current i, stored and discharged energy during the discharge process for different discharge power values. Besides, Figs. 5 and 6 show the variation of i, u, t, and power loss values for different discharge power values. It can be noted that for a higher discharge power value, the voltage u faster decreases, while the current and power losses increase.

Table 6. Results obtained during the discharge process for different discharge power values

P (W)	t (ms)	h	β	θ	u (V)	i (A)	E_{stored} (J)	$E_{discharge}$ (J)
100	35	2.4070191	1.14057×10^{-8}	21.350207	1.164915	89.8638	814.2162	3559.8
	36	2.0736857	2.01881×10^{-7}	18.323783	1.087172	97.0014	709.1658	3664.8
	37	1.7403524	3.57330×10^{-6}	15.267764	1.002661	106.266	603.1974	3770.8

P (W)	t (ms)	h	β	θ	u (V)	i (A)	E_{stored} (J)	$E_{discharge}$ (J)
	38	1.4070191	0.000063247	12.167201	0.909100	119.039	495.8777	3878.1
	39	1.0736857	0.001119476	8.9911329	0.802456	138.477	386.3614	3987.6
	40	0.7403524	0.019814706	5.6536284	0.673920	174.631	272.5009	4101.5
80	46	1.9081321	1.72128×10^{-8}	20.918198	1.032289	81.2023	639.3735	3734.6
	47	1.6414654	3.04667×10^{-7}	17.888185	0.961980	87.8107	555.2434	3818.8
	48	1.3747988	5.39261×10^{-6}	14.826925	0.885380	96.4507	470.3393	3903.7
	49	1.1081321	0.000095449	11.718047	0.800298	108.493	384.2863	3989.7
	50	0.8414654	0.001689446	8.5265379	0.702761	127.187	296.3239	4077.7
	51	0.5747988	0.029903154	5.1484959	0.583697	163.678	204.4215	4169.6
60	64	1.4759871	1.20419×10^{-8}	21.293250	0.901243	69.7012	487.3434	3886.7
	65	1.2759871	2.13142×10^{-7}	18.266366	0.840936	75.2550	424.3040	3949.7
	66	1.0759871	3.7726×10^{-6}	15.209673	0.775360	82.4710	360.7099	4013.3
	67	0.8759871	0.000066775	12.108048	0.702733	92.4324	296.3002	4077.7
	68	0.6759871	0.001181920	8.9300353	0.619888	107.630	230.5567	4143.4
	69	0.4759871	0.020919955	5.5876019	0.519881	136.065	162.1658	4211.8

Besides, the results obtained for the SC charging process are presented in Table 7. In this Table, the obtained results are presented for three values of the charge power in the initial time interval. It can be seen that α has a high value, and therefore for solving Lambert W equation, both the proposed solution methods can be used. Also, it is clear that the accuracy of a few digits is enough because of the physical nature of the problem solved.

Also, the results of the calculation of α, Ψ, u, and i are shown. Visualization of the results obtained is given in Figs. 7 and 8. It should be noted that the initial value u_0 was set to 1 V in the simulation of charging of the SC. The higher value of the charging current increases the voltage value, and vice versa. Also, it can be seen that the current values increase with the high values of the charging powers, and in this case, the initial value of α decreases for high values of charging power. However, α and Ψ values begin to increase overtime at the same level of charging power.

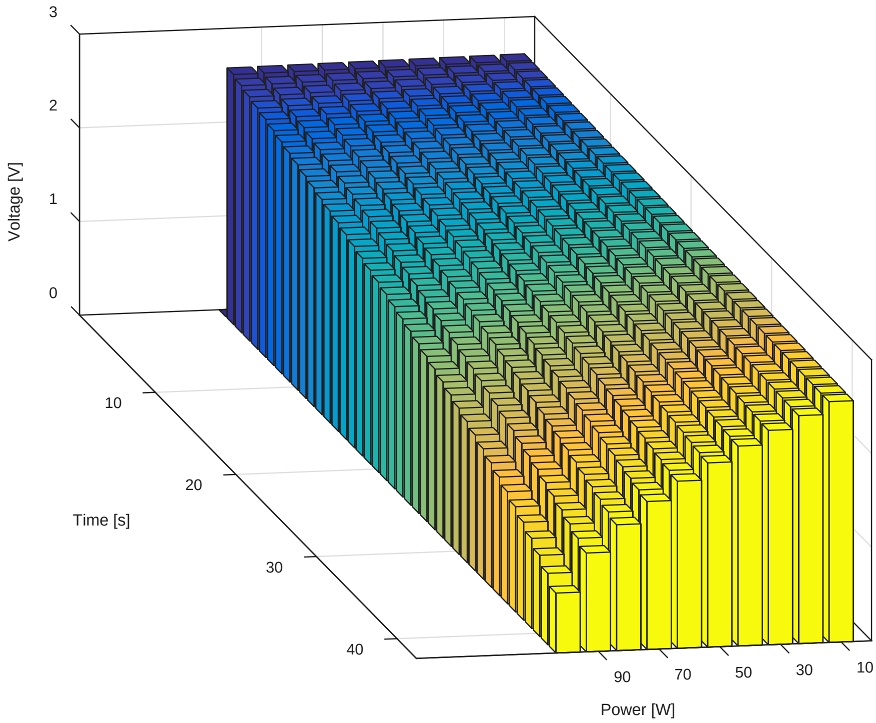

Fig. 5. Voltage changes with time for different values of power discharge

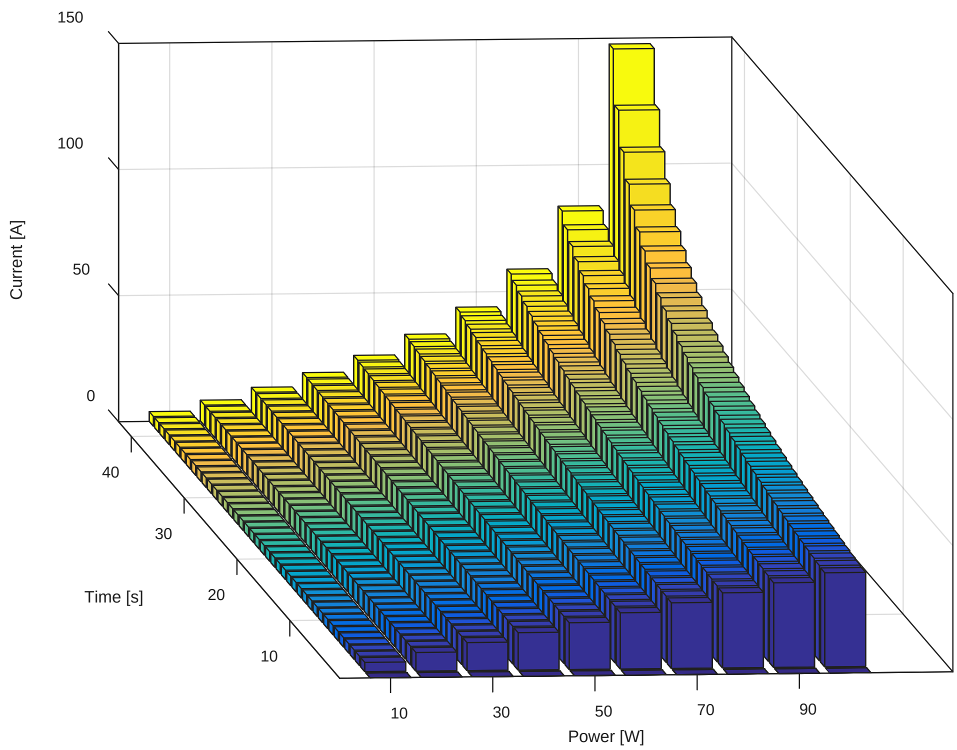

Fig. 6. Current changes with time for different values of power discharge

Table 7. Results obtained for SC charging process

P (W)	Time (s)	α	Ψ	u (V)	i (a)
	0.0	0.3922×10^6	10.5257	1.0000	180.9989
	0.1	0.5228×10^6	10.7884	1.0150	178.7816
	0.2	0.6968×10^6	11.0516	1.0298	176.6395
	0.3	0.9287×10^6	11.3154	1.0444	174.5685
	0.4	1.2379×10^6	11.5797	1.0589	172.5650
-200	0.5	1.6500×10^6	11.8444	1.0732	170.6255
	0.6	2.1993×10^6	12.1096	1.0873	168.7467
	0.7	2.9314×10^6	12.3753	1.1013	166.9257
	0.8	3.9073×10^6	12.6414	1.1152	165.1596
	0.9	5.2080×10^6	12.9079	1.1288	163.4458
	1.0	6.9418×10^6	13.1748	1.1424	161.7818
	0.0	0.2875×10^4	6.1477	1.0000	334.9348
	0.1	0.3832×10^4	6.3955	1.0276	328.3811
	0.2	0.5108×10^4	6.6447	1.0547	322.1660
	0.3	0.6808×10^4	6.8950	1.0813	316.2628
	0.4	0.9074×10^4	7.1466	1.1075	310.6474
-400	0.5	1.2095×10^4	7.3992	1.1331	305.2984
	0.6	1.6121×10^4	7.6528	1.1583	300.1962
	0.7	2.1488×10^4	7.9074	1.1832	295.3234
	0.8	2.8641×10^4	8.1630	1.2076	290.6640
	0.9	3.8176×10^4	8.4194	1.2316	286.2034
	1.0	5.0885×10^4	8.6767	1.2553	281.9286
	0.0	0.4916×10^3	4.6589	1.0000	471.2148
	0.1	0.6553×10^3	4.8965	1.0388	459.6394
	0.2	0.8734×10^3	5.1361	1.0766	448.7909
	0.3	1.1642×10^3	5.3775	1.1136	438.6011
	0.4	1.5517×10^3	5.6207	1.1497	429.0099
-600	0.5	2.0683×10^3	5.8654	1.1851	419.9642
	0.6	2.7568×10^3	6.1116	1.2198	411.4173
	0.7	3.6746×10^3	6.3593	1.2537	403.3272
	0.8	4.8979×10^3	6.6082	1.2870	395.6569
	0.9	6.5284×10^3	6.8584	1.3196	388.3731
	1.0	8.7017×10^3	7.1098	1.3517	381.4460

Other closed-form expressions of crucial key performance metrics as the state of charge (SoC) and power loss (P_{loss}) are derived for SC discharging and charging.

Firstly, the mathematical expressions for the SOC and P_{loss} are given in Eqs. (36) and (37) for the SC discharge process at constant P.

$$SOC = \frac{e_{stored}}{e_{\max}} = \frac{PR}{U_N^2}\left(2+\theta+\frac{1}{\theta}\right) \tag{36}$$

$$P_{loss} = \frac{P}{\theta} \tag{37}$$

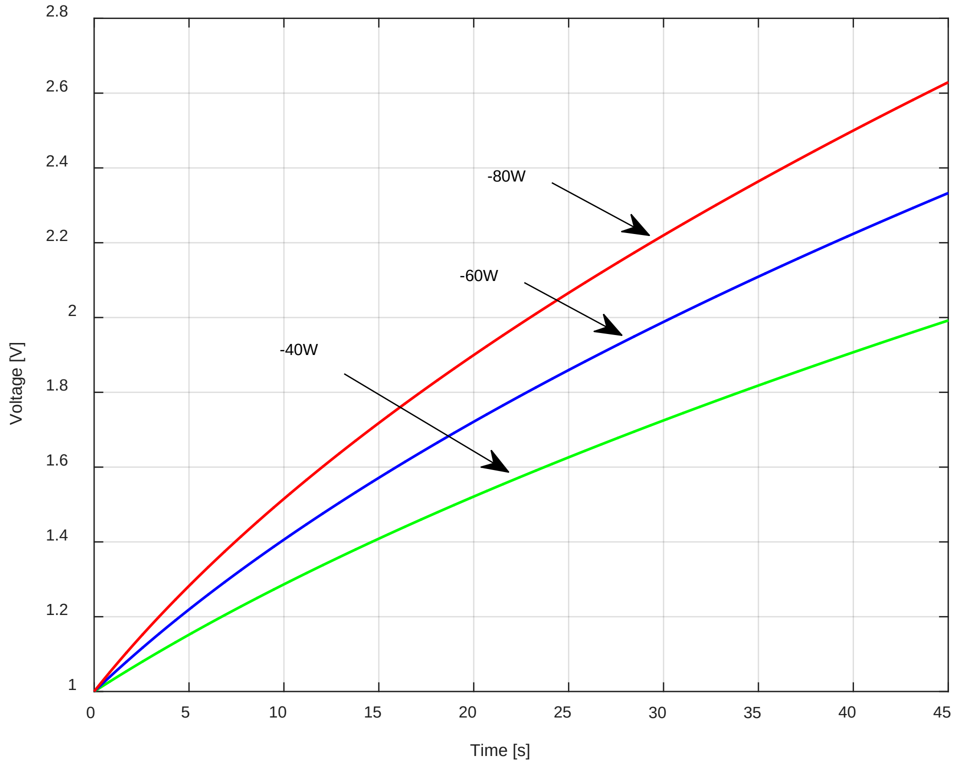

Fig. 7. Change of voltage versus time for different value of charging power

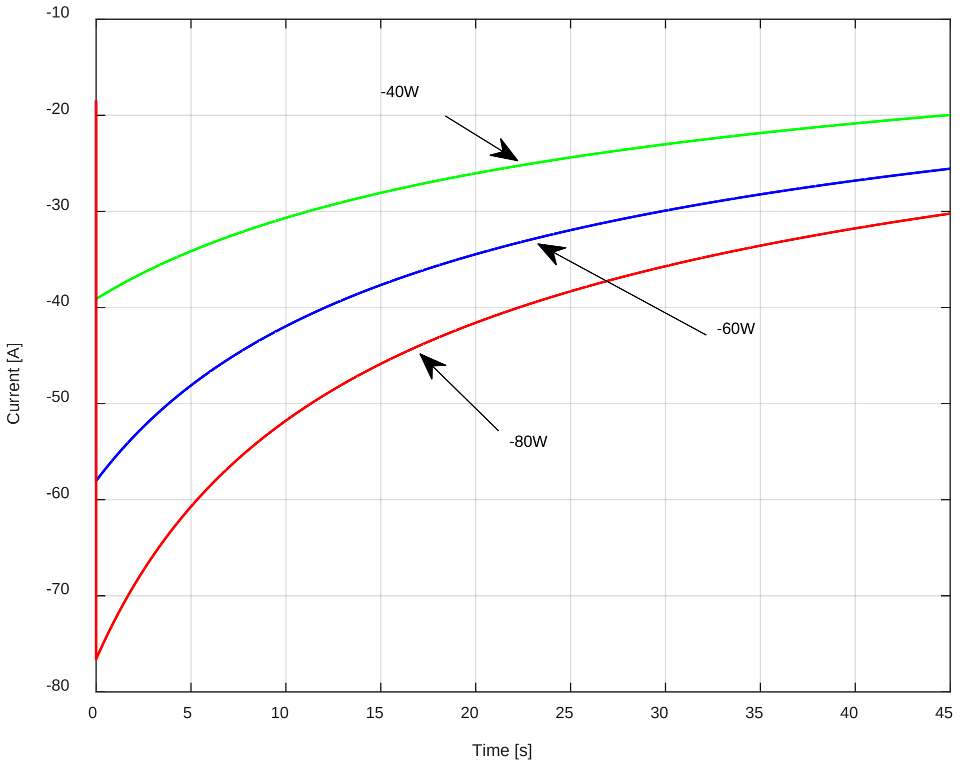

Fig. 8. Change of current versus time for different values of charging power

Figs. 9 and 10 show the SOC and P_{loss} values for different discharge power values. It can be noted that the current and power losses increase for a higher discharge power value, and the SOC rapidly decreases with time.

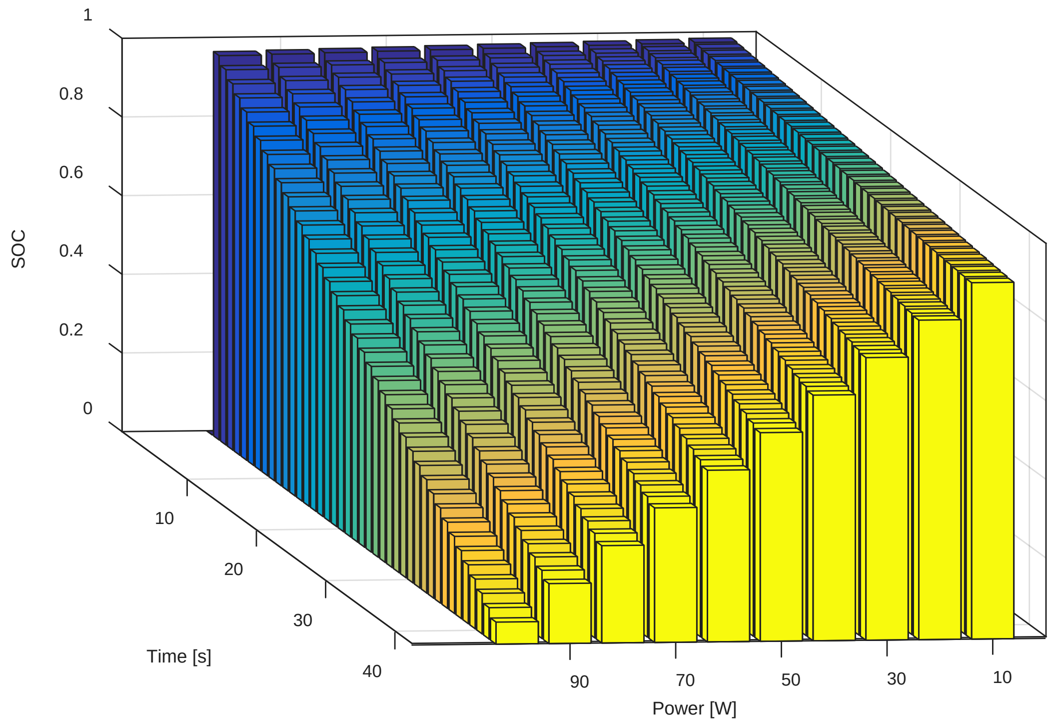

Fig. 9. SOC change with time for different values of power during SC discharge

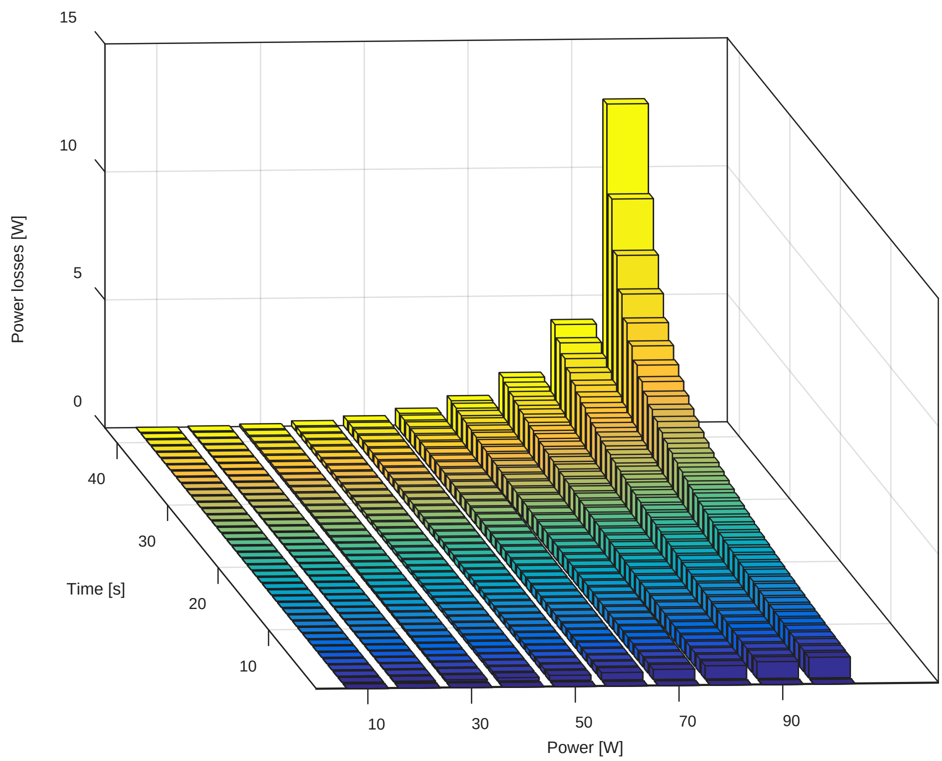

Fig. 10. Power losses change with time for different values of power during SC discharge

Secondly, the mathematical expressions for the SOC and P_{loss} are given in Eqs. (38) and (39) for the SC charge process at constant P_1.

$$SOC = \frac{e_{stored}}{e_{\max}} = \frac{P_1 R}{U_N^2} \frac{\left(\Psi - 1\right)^2}{\Psi} \tag{38}$$

$$P_{loss} = \frac{P_1}{\Psi} \tag{39}$$

Figs. 11 and 12 illustrate the SOC and P_{loss} values for different charge power values. It can be noted that the current and power losses considerably increase for a higher charge power value, and the SOC rapidly increases with time.

Thirdly, the expressions proposed in this work enable accurate estimating of the investigated metrics as SOC and P_{loss} under different conditions or parameters' variations. For illustration, Figs. 13 and 14 show the SOC and P_{loss} values during SC discharge at constant P set to 100 W, U_0 set to 2.7 V, C=1200 F, and various internal resistance values ranging from 0.4 to 0.7 mΩ.

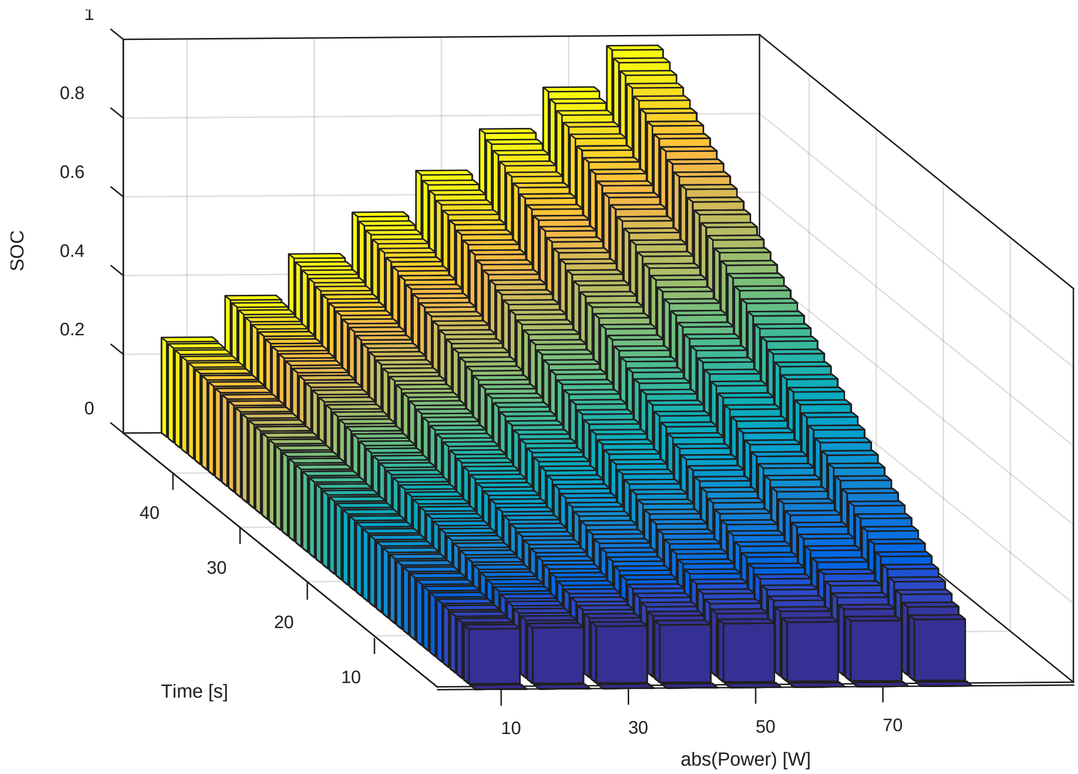

Fig. 11. SOC change with time for different values of power while charging the tested SC

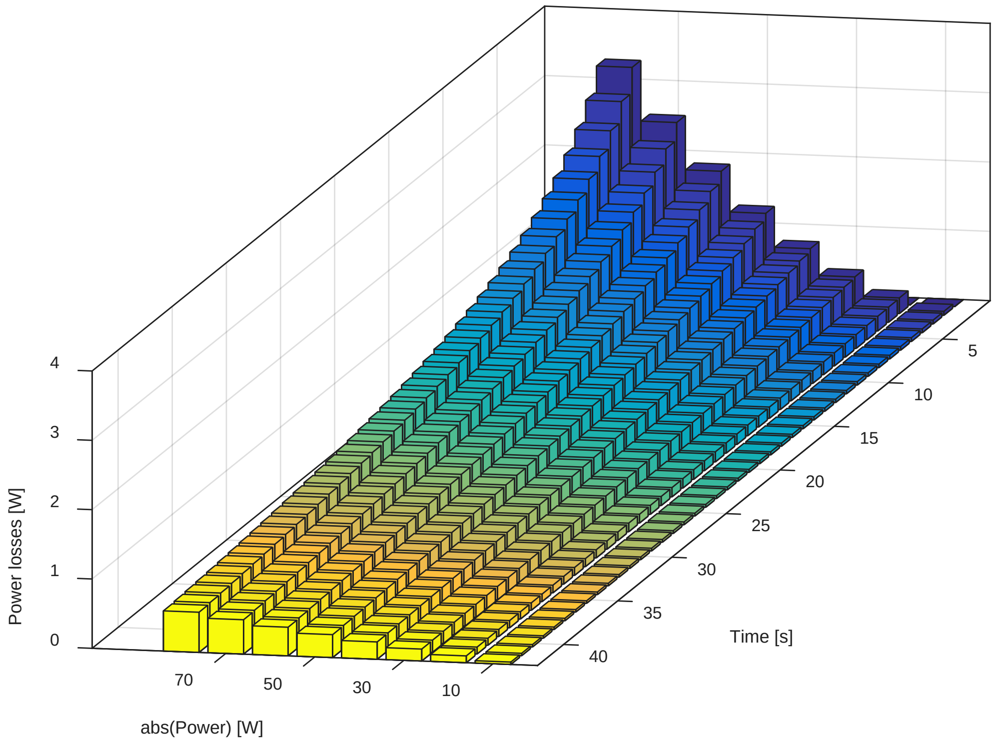

Fig. 12. Power losses change with time for different values of power while charging the tested SC

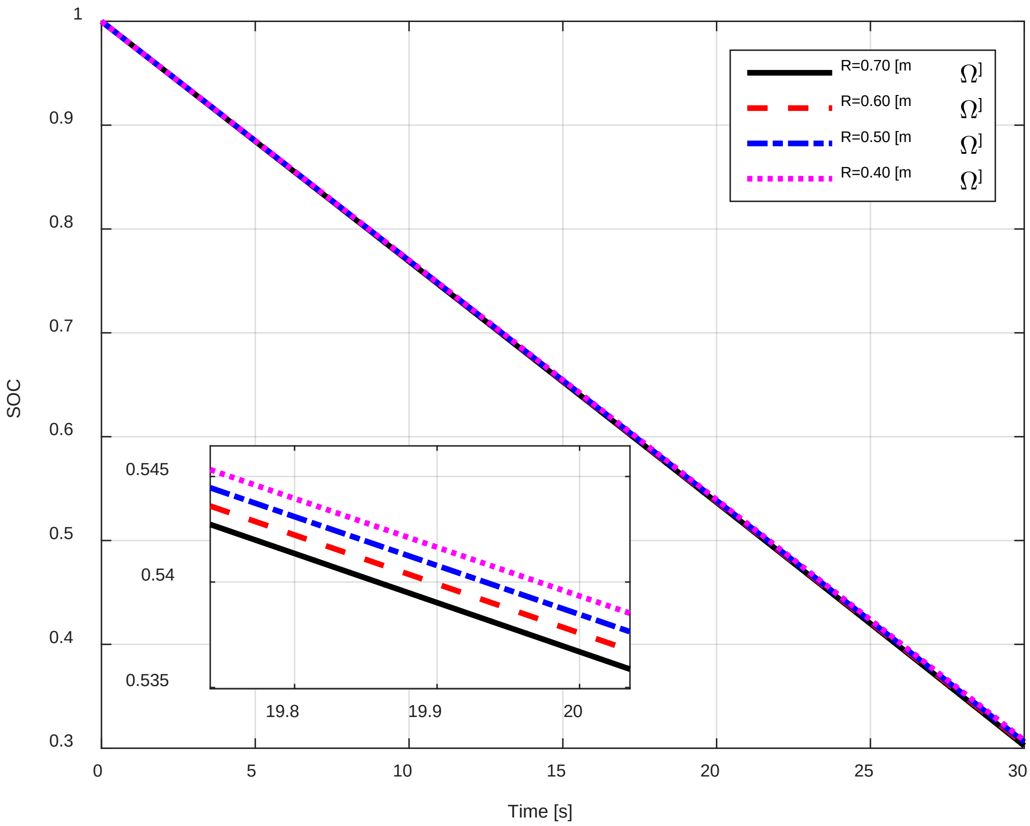

Fig. 13. SOC versus time with different *R* values during SC discharge

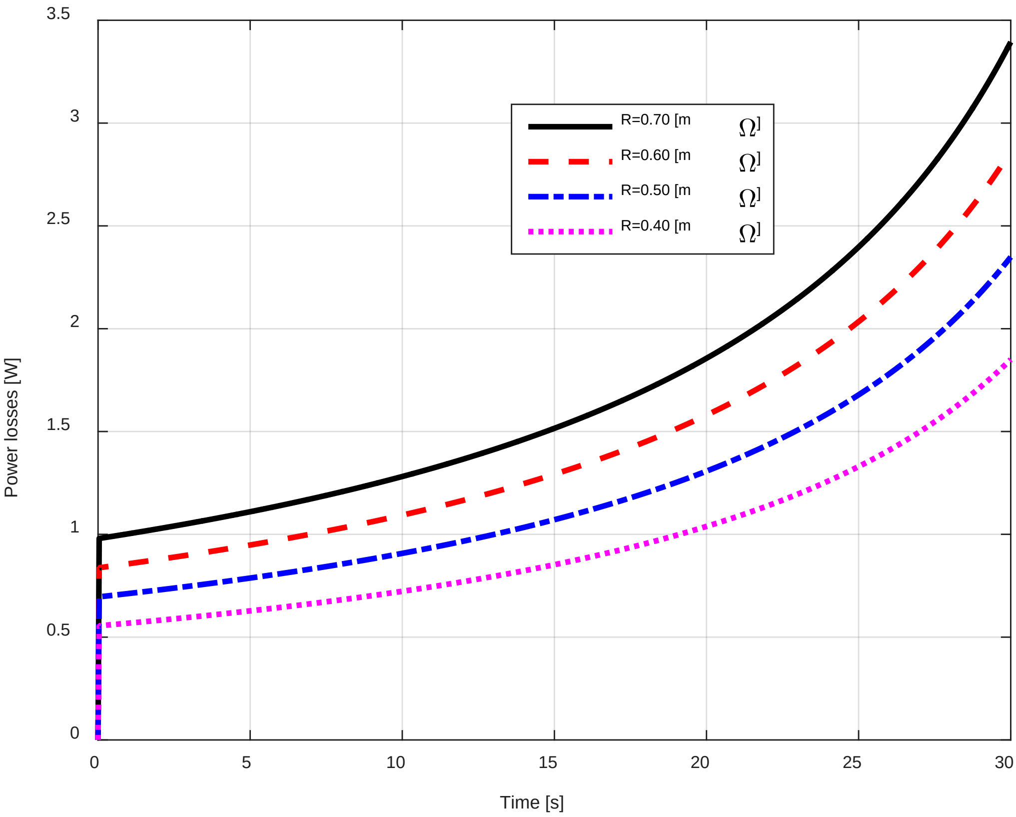

Fig. 14. Power losses versus time with different *R* values during SC discharge

Besides, Figs. 15 and 16 show the SOC and P_{loss} values during SC discharge at constant *P* set to 100 W, U_0 set to 2.7 V, *R*=0.58 mΩ, and various capacitance values ranging from 1000 to 1400 F.

Also, Figs. 17 and 18 show the SOC and P_{loss} values during SC charge at constant *P* set to 100 W, U_0 set to 1.0 V, *C*=1200 F, and various internal resistance values ranging from 0.4 to 0.7 mΩ. In addition, Figs. 19 and 20 show the SOC and P_{loss} values during SC charging at constant *P* set to 100 W, U_0 set to 1.0 V, *R*=0.58 mΩ, and various capacitance values ranging from 1000 to 1400 F.

It can be noted from Figs. 13 – 16 that when the *R*-value increases, the SOC tends to decrease, while the power losses increase at the same *C*. However, when the *C*-value decreases, the SOC decreases, while the power losses increase at the same *R*. Similarly, it is realized from Figs. 17 – 20 that when the *R*-value decreases, the SOC increases and the power losses decrease at the same *C*. However, when the *C*-value increases, the SOC decreases, while the power losses increase at the same *R*.

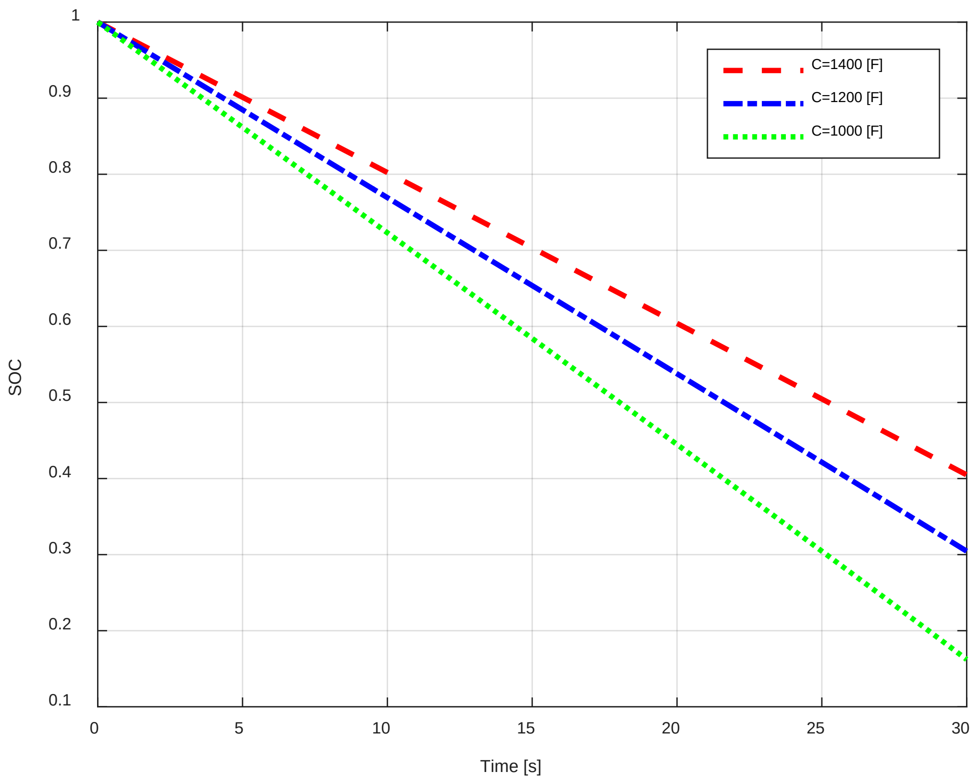

Fig. 15. SOC versus time with different capacitance values during SC discharge

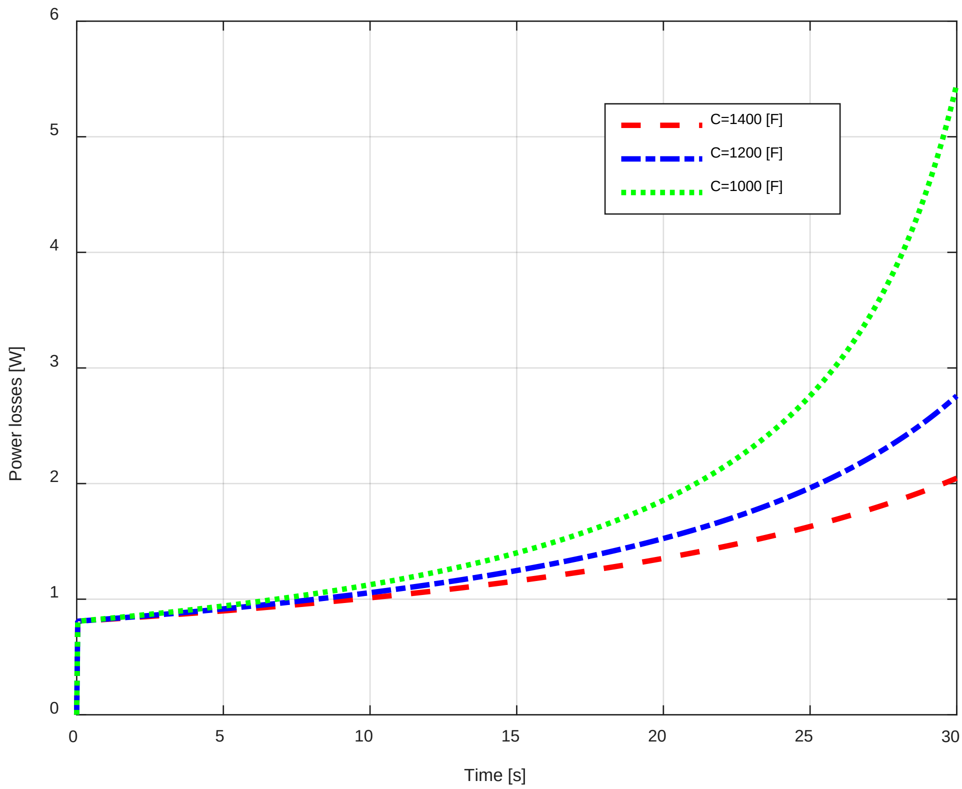

Fig. 16. Power losses versus time with different capacitance values during SC discharge

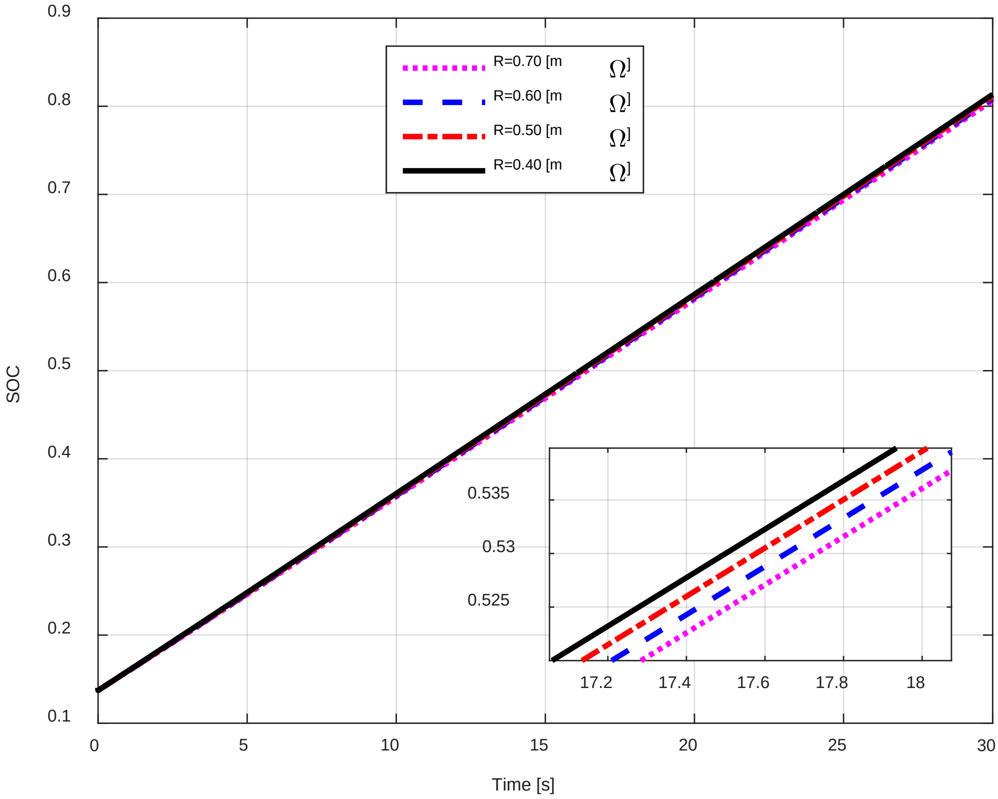

Fig. 17. SOC versus time with different *R* values during SC charging

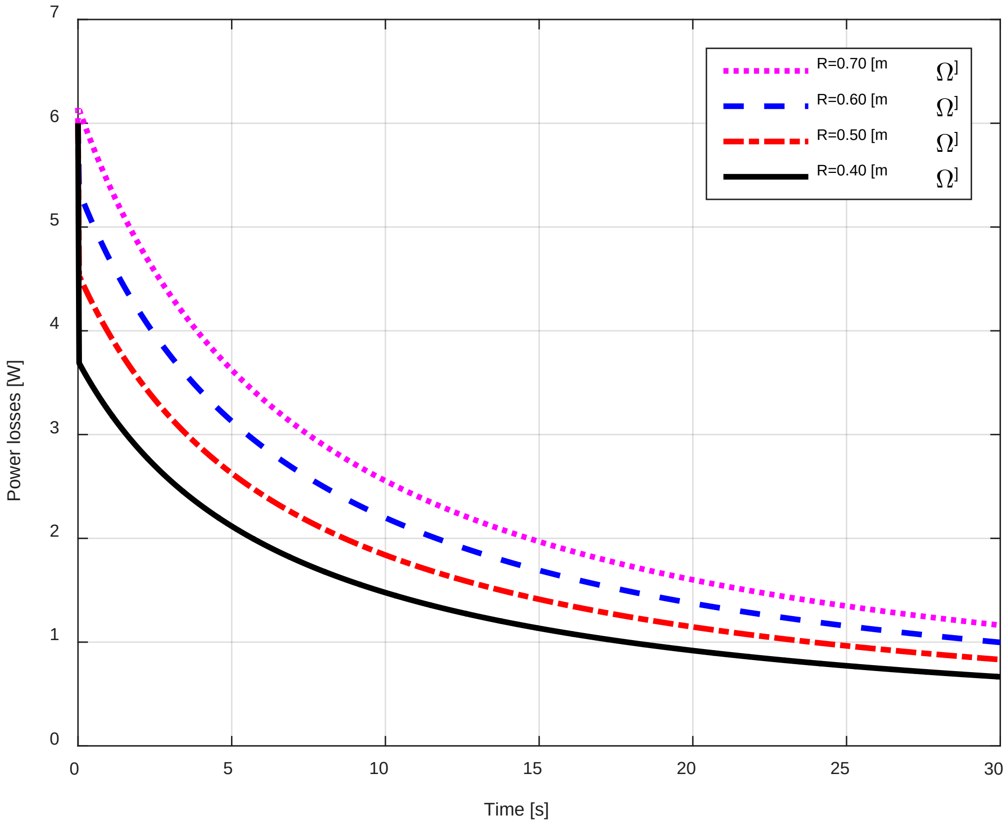

Fig. 18. Power losses versus time with different *R* values during SC charging

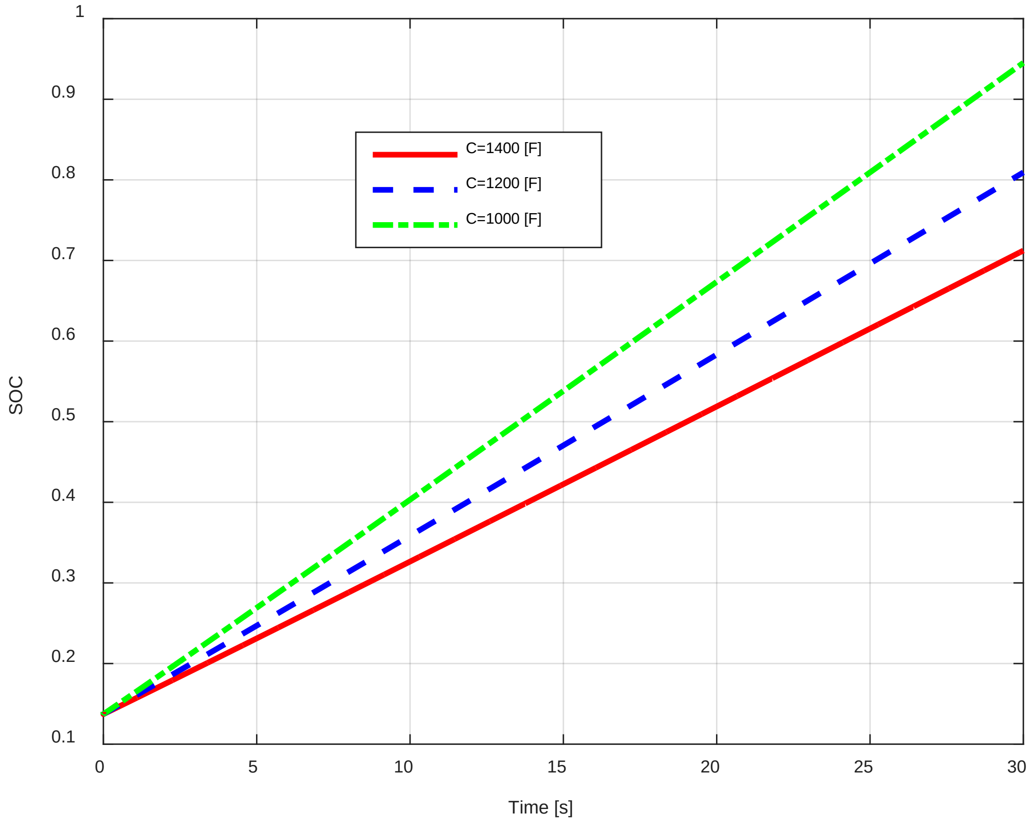

Fig. 19. SOC versus time with different capacitance values during SC charging

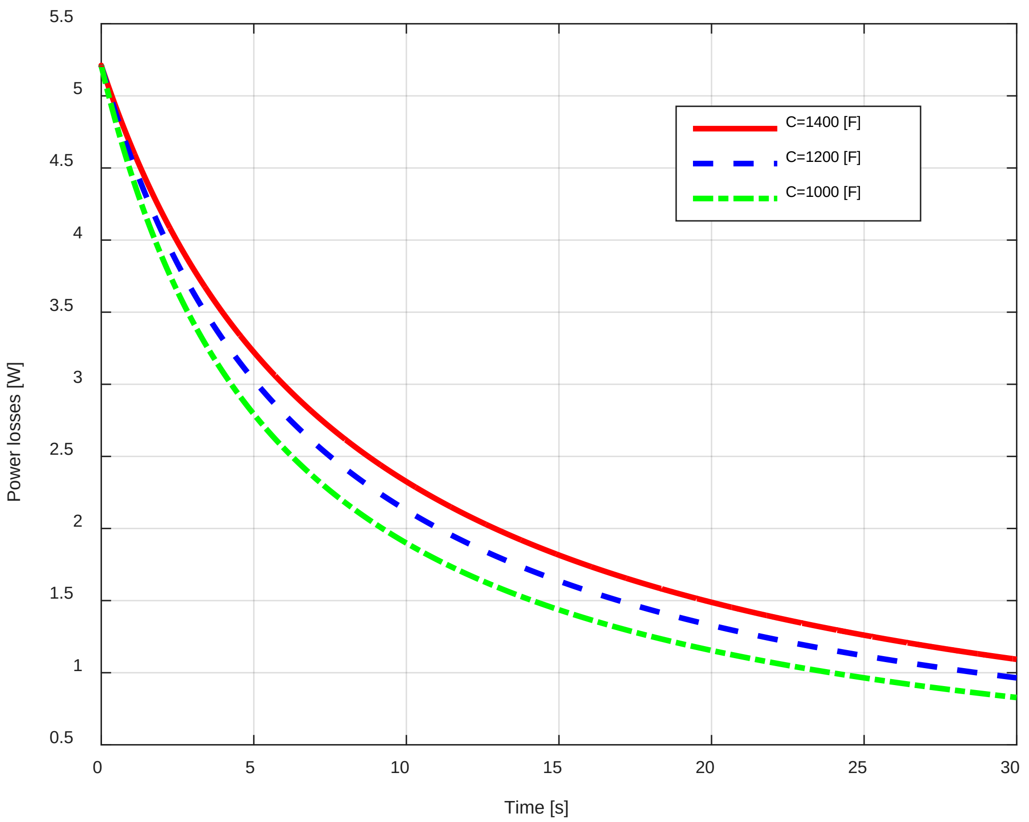

Fig. 20. Power losses versus time with different capacitance values during SC charging

5. Conclusions

In this work, a mathematical time-domain analysis that enables the explicit finding of the electrical variables involved in the charge/discharge processes of SCs – voltage, current, power, energy, SOC, and P_{loss} – operated at constant power is investigated. The mathematical expressions for these variables are transcendental. In the literature, transcendental equations are rarely solved using iterative methods. The discharge process of SCs operating at constant power can be represented as a function of the type $\theta = \beta \exp(\theta)$. This equation has two solutions. However, taking into account the physical constraints, only one is acceptable. Also, the charging process of SCs operating at constant power can be represented as a function of the type $\Psi = \alpha \exp(-\Psi)$ which also has one solution. In this regard, the analytical solutions for the charging and discharging equations are derived in the form of the Lagrange inversion theorem of the Lambert W function in its asymptotic formula and the form of STFT.

Furthermore, numerical results obtained by using all mentioned methods are presented. The mathematical expressions derived are accurate and straightforward and do not require any other mathematical formulations. Comprehensive simulation results obtained at the parametric variation of the parameters are presented to demonstrate the proposed equations' applicability and accuracy. The closed-form expressions suggested in this paper are accurate and straightforward, which can advance a good base for proper modeling, investigation, sizing, regulation, and controlling constant power SCs in modern energy systems.

Our future research will focus on the mathematical description of SCs' charging and discharging in practical applications under different modes of operation.

Appendix A

Derivation of Eq. (11): the internal voltage expression

One can consider the combinatorial variable z as given in Eq. (A.1); thus Eq. (7) can be rewritten as given in Eq. (A.2):

$$z = u + \sqrt{u^2 - 4PR} \tag{A.1}$$

$$z^2 + 4PR - 4PR\log\left(z^2\right) = 2h \tag{A.2}$$

Also, one can consider the combinatorial variable y as given in Eq. (A.3), then Eq. (A.2) can be rewritten as given in Eq. (A.4):

$$y = z^2 + 4PR - 2h \tag{A.3}$$

$$e^{\frac{y}{4PR}} = y + 2h - 4PR \tag{A.4}$$

Hence, one can reformulate Eq. (A.4) as follows:

$$\frac{1}{4PR} e^{\frac{y+2h-4PR}{4PR}} e^{-\frac{2h-4PR}{4PR}} = \frac{y+2h-4PR}{4PR} \tag{A.5}$$

Thus:

$$\begin{aligned} \beta &= \frac{1}{4PR} e^{\frac{4PR-2h}{4PR}} \\ \theta &= \frac{y+2h-4PR}{4PR} \end{aligned} \tag{A.6}$$

Finally, from Eqs. (A.1)- (A.6), one can derive u expression as follows:

$$\begin{aligned} u &= \frac{z^2 + 4PR}{2z} \\ u &= \frac{y+2h}{2\sqrt{y+2h-4PR}} \\ u &= \frac{y+2h-4PR+4PR}{2\sqrt{y+2h-4PR}} \\ u &= \frac{4PR\theta + 4PR}{2\sqrt{4PR\theta}} \\ u &= \sqrt{PR}\left(\frac{1+\theta}{\sqrt{\theta}}\right) \end{aligned} \tag{A.7}$$

Derivation of Eq. (13): the discharge current expression.

The discharge current can be expressed as given in Eq. (12). Substituting Eq. (A.7) into Eq. (12), thus:

$$\frac{du}{d\theta}=\sqrt{PR}\left(\frac{\sqrt{\theta}-(1+\theta)\frac{1}{2\sqrt{\theta}}}{\theta}\right)=\sqrt{PR}\left(\frac{\theta-1}{2\theta\sqrt{\theta}}\right) \quad \text{(A.8)}$$

Also, one can express $\frac{d\theta}{dt}$ as follows:

$$\frac{d\theta}{dt}=\frac{d\theta}{d\beta}\frac{d\beta}{dt} \quad \text{(A.9)}$$

As $\theta=\beta\exp(\theta)$, *i.e.*, $\theta\exp(-\theta)=\beta$, one can write the following expression

$$\begin{aligned}
&\theta' e^{-\theta}-\theta e^{-\theta}\theta'=1\\
&\theta'=\frac{1}{e^{-\theta}-\theta e^{-\theta}}=\frac{1}{e^{-\theta}-\beta}=\frac{1}{\frac{\beta}{\theta}-\beta}=\frac{\theta}{\beta(1-\theta)}
\end{aligned} \quad \text{(A.10)}$$

On the other side, as $\beta=\frac{1}{4PR}e^{\frac{4PR-2h}{4PR}}$, one can derive the following expressions

$$\begin{aligned}
&\frac{d\beta}{dt}=\frac{1}{4PR}e^{\frac{4PR-2h}{4PR}}\left(\frac{1}{2PR}\right)\left(\frac{4P}{C}\right)\\
&\frac{d\beta}{dt}=\beta\left(\frac{2}{RC}\right)
\end{aligned} \quad \text{(A.11)}$$

Hence, one can derive the current expression as follows:

$$\begin{aligned}
&i=C\left(\frac{du}{d\theta}\right)\left(\frac{d\theta}{dt}\right)\\
&i=C\left[\left(\sqrt{PR}\frac{\theta-1}{2\theta\sqrt{\theta}}\right)\right]\left[\left(\frac{\theta}{\beta(1-\theta)}\right)\left(\beta\frac{2}{RC}\right)\right]\\
&i=-\sqrt{\frac{P}{R\theta}}
\end{aligned} \quad \text{(A.12)}$$

where the negative sign in Eq. (A.12) indicates the discharge process.

Derivation of Eq. (20): the voltage during charging expression

During a charging process, the power is less than zero. Hence, one can consider P_1=-P. One can consider the combinatorial variable z as given in Eq. (A.13); thus Eq. (17) can be rewritten as given in Eq. (A.14):

$$z=u+\sqrt{u^2-4PR} \quad \text{(A.13)}$$

$$z^2-4P_1R+4P_1R\log\left(z^2\right)=2h \quad \text{(A.14)}$$

Also, one can consider the combinatorial variable *y* as given in Eq. (A.15), then Eq. (A.14) can be rewritten as given in Eq. (A.16):

$$y = z^2 - 4P_1R - 2h \tag{A.15}$$

$$e^{-\frac{y}{4P_1R}} = y + 2h + 4P_1R \tag{A.16}$$

Hence;

$$\frac{1}{4P_1R} e^{-\frac{y+2h+4P_1R}{4P_1R}} e^{\frac{2h+4P_1R}{4P_1R}} = \frac{y+2h+4P_1R}{4P_1R} \tag{A.17}$$

Thus:

$$\begin{aligned} \alpha &= \frac{1}{4P_1R} e^{\frac{4P_1R+2h}{4P_1R}} \\ \psi &= \frac{y+2h+4P_1R}{4P_1R} \end{aligned} \tag{A.18}$$

As $z = u + \sqrt{u^2 + 4P_1R}$ then;

$$\begin{aligned} u &= \frac{z^2 - 4P_1R}{2z} \\ u &= \frac{y+2h}{2\sqrt{y+2h+4P_1R}} \\ u &= \frac{y+2h+4P_1R-4P_1R}{2\sqrt{y+2h+4P_1R}} \\ u &= \frac{4P_1R\psi - 4P_1R}{2\sqrt{4P_1R\psi}} \\ u &= \sqrt{PR}\left(\frac{\psi-1}{\sqrt{\psi}}\right) \end{aligned} \tag{A.19}$$

Derivation of Eq. (21): the charging current expression.

From Eq. (A.19), one can find that:

$$\frac{du}{d\psi} = \sqrt{P_1R}\left(\frac{\sqrt{\psi} - (\psi-1)\frac{1}{2\sqrt{\psi}}}{\psi}\right) = \sqrt{P_1R}\left(\frac{\psi+1}{2\psi\sqrt{\psi}}\right) \tag{A.20}$$

Also, one can distribute $\frac{d\psi}{dt}$ as follows:

$$\frac{d\psi}{dt} = \frac{d\psi}{d\alpha}\frac{d\alpha}{dt} \tag{A.21}$$

Now, as $\psi = \alpha\exp(-\psi)$, *i.e.*, $\psi\exp(\psi) = \alpha$ .Thus:

$$\psi' e^{\psi} + \psi e^{\psi} \psi' = 1$$
$$\psi' = \frac{1}{e^{\psi} + \psi e^{\psi}} = \frac{1}{e^{\psi} + \alpha} = \frac{1}{\frac{\psi}{\alpha} + \alpha} = \frac{\psi}{\alpha(\psi+1)} \tag{A.22}$$

On the other side, as $\alpha = \frac{1}{4P_1R} e^{\frac{4P_1R+2h}{4P_1R}}$, one can write the following:

$$\frac{d\alpha}{dt} = \frac{1}{4P_1R} e^{\frac{4P_1R+2h}{4P_1R}} \left(\frac{1}{2P_1R}\right)\left(\frac{4P_1}{C}\right)$$
$$\frac{d\alpha}{dt} = \alpha \frac{2}{RC} \tag{A.23}$$

Hence, one can derive the current expression as follows:

$$i = C\left(\frac{du}{d\psi}\right)\left(\frac{d\psi}{dt}\right)$$
$$i = C\left(\sqrt{P_1R}\,\frac{\psi+1}{2\psi\sqrt{\psi}}\right)\left(\frac{\psi}{\alpha(\psi+1)}\right)\left(\alpha\frac{2}{RC}\right) \tag{A.24}$$
$$i = \sqrt{\frac{P_1}{\psi R}}$$

Appendix B

B.1 Mathematica code for expressing the discharging process of a SC at constant power

For solving $\theta = \beta \exp(\theta)$, the following Mathematica code can be used.

```
NumberOFdigits = 1000;
bet = 1 / 10
x = 35;
```

$$\text{Fmanje} = \sum_{m=0}^{x} (-1)\,\hat{}\,m * \text{bet}\,\hat{}\,m * ((x - m)\,\hat{}\,m) / m!;$$

$$\text{Fmanje1} = \sum_{m=0}^{x+1} (-1)\,\hat{}\,m * \text{bet}\,\hat{}\,m * ((x + 1 - m)\,\hat{}\,m) / m!;$$

```
ThetaLOWER = bet * (Fmanje / Fmanje1);
ErrorThetaLOWER = Abs[ThetaLOWER – bet * E ^ ThetaLOWER];
Print["ThetaLOWER= ", SetPrecision[ThetaLOWER, NumberOFdigits]];
Print["ErrorThetaLOWER= ", SetPrecision[ErrorThetaLOWER, NumberOFdigits]];

a = 2 * Log[3];
b = ThetaLOWER / a;
U = 200 * a;
```

$$R = \sum_{m=0}^{\text{IntegerPart}[U/a]} (((-1)\,\hat{}\,m) * (b\,\hat{}\,m) * (E\,\hat{}\,(-a * b * m)) * ((U - m * a)\,\hat{}\,m) / m!);$$

$$Ra = \sum_{m=0}^{\text{IntegerPart}[(U-a)/a]} (((-1)\,\hat{}\,m) * (b\,\hat{}\,m) * (E\,\hat{}\,(-a * b * m)) * ((U - a - m * a)\,\hat{}\,m) / m!);$$

$$R2a = \sum_{m=0}^{\text{IntegerPart}[(U-2*a)/a]} (((-1)\,\hat{}\,m) * (b\,\hat{}\,m) * (E\,\hat{}\,(-a * b * m)) * ((U - 2 * a - m * a)\,\hat{}\,m) / m!);$$

```
Fvece = b * E ^ (b * U) * (R – (E ^ (–a * b)) * Ra);
Fvece1 = b * E ^ (b * (U – a)) * (Ra – (E ^ (–a * b)) * R2a);

K = Log[(Fvece1 / Fvece)];
ThetaUPPER = K + ThetaLOWER;

ErrorThetaUPPER = Abs[ThetaUPPER – bet * E ^ ThetaUPPER];

Print["ThetaUPPER= ", SetPrecision[ThetaUPPER, brojcifara]];
Print["ErrorThetaUPPER= ", SetPrecision[ErrorThetaUPPER, brojcifara]];
```

B.2 Mathematica code for expressing the charging process of a SC at constant power

For solving $\Psi = \alpha \exp(-\Psi)$, Lambert W equation, the following Mathematica code can be used.

```
digitnumber = 500;
B = 1/1000;
Print["B= ", B];
M = 50;
Print["M= ", M];
```

$$F1 = \sum_{n=0}^{M} (B \wedge n * (((M - n) \wedge n) / n!));$$

$$F2 = \sum_{n=0}^{M+1} (B \wedge n * (((M + 1 - n) \wedge n) / n!));$$

```
SolutionTRANS = SetPrecision[B*(F1/F2), digitnumber];
Print["SolutionTRANS= ", SolutionTRANS]
ErrorTRANS = SetPrecision[Abs[SolutionTRANS - B*E^(-SolutionTRANS)], digitnumber];
Print["ErrorTRANS= ", ErrorTRANS]
```

$$\text{solutionLAMBERT} = \sum_{NNN=1}^{M} (B \wedge NNN * (((NNN) \wedge (NNN - 1)) / NNN!));$$

```
Print["solutionLAMBERT= ", SetPrecision[solutionLAMBERT, digitnumber]];
ErrorLAMBERT = SetPrecision[Abs[solutionLAMBERT - B*E^(-solutionLAMBERT)], digitnumber];
Print["ErrorLAMBERT= ", ErrorLAMBERT]

L1 = Log[B];
L2 = Log[L1];
```

$$\text{largeLambert} = L1 - L2 + \sum_{l=0}^{M} \sum_{k=1}^{M} (((-1) \wedge l * \text{StirlingS1}[l + k, l + 1] * L1 \wedge (-l - k) * L2 \wedge k \;)/k!);$$

```
largeLambert = L1 - L2 + Sum[(((-1)^j*Abs[StirlingS1[j + k, j + 1]]*L1^(-j - k)*L2^k )/k!), {j, 0, M}, {k, 1, M}];

Print["solutionlagreLambert= ", SetPrecision[largeLambert, digitnumber]];
ErrorlagreLambert = SetPrecision[Abs[largeLambert - B*E^(-largeLambert)], digitnumber];
Print["ErrorlagreLambert= ", ErrorlagreLambert]
```


Funding sources

This research did not receive any specific grant from funding agencies in the public, commercial, or not-for-profit sectors.

References

[1] S.H.E. Abdel Aleem, A.F. Zobaa, H.M. Abdel Mageed, Assessment of energy credits for the enhancement of the Egyptian Green Pyramid Rating System, Energy Policy. 87 (2015) 407–416. doi:10.1016/j.enpol.2015.09.033.

[2] M.H. Mostafa, S.H.E.A. Aleem, S.G. Ali, A.Y. Abdelaziz, P.F. Ribeiro, Z.M. Ali, Robust energy management and economic analysis of microgrids considering different battery characteristics, IEEE Access. 8 (2020) 54751–54775. doi:10.1109/ACCESS.2020.2981697.

[3] S. Lepszy, Analysis of the storage capacity and charging and discharging power in energy storage systems based on historical data on the day-ahead energy market in Poland, Energy. 213 (2020) 118815. doi:10.1016/j.energy.2020.118815.

[4] N.V. Quynh, Z.M. Ali, M.M. Alhaider, A. Rezvani, K. Suzuki, Optimal energy management strategy for a renewable-based microgrid considering sizing of battery energy storage with control policies, Int. J. Energy Res. 45 (2021) 5766–5780. doi:10.1002/er.6198.

[5] M.H. Mostafa, S.H.E. Abdel Aleem, S.G. Ali, Z.M. Ali, A.Y. Abdelaziz, Techno-economic assessment of energy storage systems using annualized life cycle cost of storage (LCCOS) and levelized cost of energy (LCOE) metrics, J. Energy Storage. 29 (2020) 101345. doi:10.1016/j.est.2020.101345.

[6] M. Khosravi, S. Afsharnia, S. Farhangi, Optimal sizing and technology selection of hybrid energy storage system with novel dispatching power for wind power integration, Int. J. Electr. Power Energy Syst. 127 (2021) 106660. doi:10.1016/j.ijepes.2020.106660.

[7] M.S. Guney, Y. Tepe, Classification and assessment of energy storage systems, Renew. Sustain. Energy Rev. 75 (2017) 1187–1197. doi:10.1016/j.rser.2016.11.102.

[8] W. Jing, C.H. Lai, S.H.W. Wong, M.L.D. Wong, Battery-supercapacitor hybrid energy storage system in standalone DC microgrids: A review, IET Renew. Power Gener. 11 (2017) 461–469. doi:10.1049/iet-rpg.2016.0500.

[9] A. Kuperman, I. Aharon, Battery-ultracapacitor hybrids for pulsed current loads: A review, Renew. Sustain. Energy Rev. 15 (2011) 981–992. doi:10.1016/j.rser.2010.11.010.

[10] S. Lemofouet, A. Rufer, Hybrid energy storage systems based on compressed air and supercapacitors with maximum efficiency point tracking, in: 2005 Eur. Conf. Power Electron. Appl., IEEE, 2005: pp. 10 pp.-P.10. doi:10.1109/epe.2005.219203.

[11] F. Naseri, E. Farjah, T. Ghanbari, An efficient regenerative braking system based on battery/supercapacitor for electric, hybrid, and plug-in hybrid electric vehicles with BLDC motor, IEEE Trans. Veh. Technol. 66 (2017) 3724–3738. doi:10.1109/TVT.2016.2611655.

[12] C. Abbey, G. Joos, Supercapacitor energy storage for wind energy applications, IEEE Trans. Ind. Appl. 43 (2007) 769–776. doi:10.1109/TIA.2007.895768.

[13] L. Qu, W. Qiao, Constant power control of DFIG wind turbines with supercapacitor energy storage, IEEE Trans. Ind. Appl. 47 (2011) 359–367. doi:10.1109/TIA.2010.2090932.

[14] A. Lahyani, P. Venet, A. Guermazi, A. Troudi, Battery/Supercapacitors Combination in Uninterruptible Power Supply (UPS), IEEE Trans. Power Electron. 28 (2013) 1509–1522. doi:10.1109/TPEL.2012.2210736.

[15] R. Chai, Y. Zhang, A Practical Supercapacitor Model for Power Management in Wireless Sensor Nodes, IEEE Trans. Power Electron. 30 (2015) 6720–6730. doi:10.1109/TPEL.2014.2387113.

[16] Z. Li, X. Huang, K. Song, J. Jiang, C. Zhu, Z. Du, Constant Current Charging and the Maximum System Efficiency Tracking for Wireless Charging Systems Employing Dual-side Control, 2018 Int. Power Electron. Conf. IPEC-Niigata - ECCE Asia 2018. 33 (2018) 84–87. doi:10.23919/IPEC.2018.8507468.

[17] A.S. Elwakil, A. Allagui, B.J. Maundy, C. Psychalinos, A low frequency oscillator using a super-capacitor, AEU - Int. J. Electron. Commun. 70 (2016) 970–973. doi:10.1016/j.aeue.2016.03.020.

[18] L. Zhang, X. Hu, Z. Wang, F. Sun, D.G. Dorrell, A review of supercapacitor modeling, estimation, and applications: A control/management perspective, Renew. Sustain. Energy Rev. 81 (2018) 1868–1878. doi:10.1016/j.rser.2017.05.283.

[19] A. Fathy, H. Rezk, Robust electrical parameter extraction methodology based on Interior Search Optimization Algorithm applied to supercapacitor, ISA Trans. 105 (2020) 86–97. doi:10.1016/j.isatra.2020.05.016.

[20] P.J. Grbović, P. Delarue, P. Le Moigne, P. Bartholomeus, Modeling and control of the ultracapacitor-based regenerative controlled electric drives, IEEE Trans. Ind. Electron. 58 (2011) 3471–3484. doi:10.1109/TIE.2010.2087290.

[21] V. Musolino, L. Piegari, E. Tironi, New full-frequency-range supercapacitor model with easy identification procedure, IEEE Trans. Ind. Electron. 60 (2013) 112–120. doi:10.1109/TIE.2012.2187412.

[22] N. Gyawali, Y. Ohsawa, Integrating fuel cell/electrolyzer/ultracapacitor system into a stand-alone microhydro plant, IEEE Trans. Energy Convers. 25 (2010) 1092–1101. doi:10.1109/TEC.2010.2066977.

[23] H. Yu, D. Cao, Multi-objective Optimal Sizing and Real-time Control of Hybrid Energy Storage Systems for Electric Vehicles, IEEE Intell. Veh. Symp. Proc. 2018-June (2018) 191–196. doi:10.1109/IVS.2018.8500629.

[24] C. Zhao, H. Yin, Z. Yang, C. Ma, Equivalent series resistance-based energy loss analysis of a battery semiactive hybrid energy storage system, IEEE Trans. Energy Convers. 30 (2015) 1081–1091. doi:10.1109/TEC.2015.2418818.

[25] R.L. Spyker, Classical equivalent circuit parameters for a double-layer capacitor, IEEE Trans. Aerosp. Electron. Syst. 36 (2000) 829–836. doi:10.1109/7.869502.

[26] J.F. Pedrayes, M.G. Melero, J.M. Cano, J.G. Norniella, S.B. Duque, C.H. Rojas, G.A. Orcajo, Lambert W function based closed-form expressions of supercapacitor electrical variables in constant power applications, Energy. 218 (2021) 119364. doi:10.1016/j.energy.2020.119364.

[27] O. Abdel-Baqi, P. Miller, Dynamic performance improvement and peak power limiting using high power ultracapacitor system for hydraulic mining shovels, AABC 2014 - Adv. Automot. Batter. Confernce, LLIBTA Symp. Track A Cell Mater. Chem. Track B Batter. Eng. Large Lithium Ion Batter. Technol. Appl. ECCAP Symp. - Large EC Capacit. Technol. Appl. 62 (2014) 3173–3181.

[28] M. Technologies, Maxwell Technologies, 2014.

[29] M.E. Fouda, A. Allagui, A.S. Elwakil, A. Eltawil, F. Kurdahi, Supercapacitor discharge under constant resistance, constant current and constant power loads, J. Power Sources. 435 (2019) 226829. doi:10.1016/j.jpowsour.2019.226829.

[30] J.F. Gómez-Aguilar, H. Yépez-Martínez, R.F. Escobar-Jiménez, C.M. Astorga-Zaragoza, J. Reyes-Reyes, Analytical and numerical solutions of electrical circuits described by fractional derivatives, Appl. Math. Model. 40 (2016) 9079–9094. doi:10.1016/j.apm.2016.05.041.

[31] S.M. Perovich, M. Orlandic, M. Calasan, Concerning exact analytical STFT solutions to some families of inverse problems in engineering material theory, Appl. Math. Model. 37 (2013) 5474–5497. doi:10.1016/j.apm.2012.10.052.

[32] M.P. Calasan, S.M. Perovich, On an exact analytical solution in Weibull probability distribution domain, in: ENERGYCON 2014 - IEEE Int. Energy Conf., IEEE, 2014: pp. 1218–1222. doi:10.1109/ENERGYCON.2014.6850578.

[33] M. Ćalasan, S.H.E. Abdel Aleem, A.F. Zobaa, A new approach for parameters estimation of double and triple diode models of photovoltaic cells based on iterative Lambert W function, Sol. Energy. 218 (2021) 392–412. doi:10.1016/j.solener.2021.02.038.

[34] M. Ćalasan, S.H.E. Abdel Aleem, A.F. Zobaa, On the root mean square error (RMSE) calculation for parameter estimation of photovoltaic models: A novel exact analytical solution based on Lambert W function, Energy Convers. Manag. 210 (2020) 112716. doi:10.1016/j.enconman.2020.112716.

[35] M.P. Ćalasan, Analytical solution for no-load induction machine speed calculation during direct start-up, Int. Trans. Electr. Energy Syst. 29 (2019) e2777. doi:10.1002/etep.2777.

[36] M. Calasan, A. Nedic, Experimental Testing and Analytical Solution by Means of Lambert W-Function of Inductor Air Gap Length, Electr. Power Components Syst. 46 (2018) 852–862. doi:10.1080/15325008.2018.1488012.